Multiple-Symbol Joint Signal Processing for Differentially Encoded Single- and Multi-Carrier Communications: Principles, Designs and Applications

Li Wang, *Member, IEEE*, Li Li, Chao Xu, Dandan Liang, Soon Xin Ng, *SM, IEEE*, and Lajos Hanzo, *Fellow, IEEE*

***Abstract*—Bypassing the potentially excessive-complexity and yet inaccurate channel estimation, differentially encoded modulation in conjunction with low-complexity non-coherent detection constitutes a viable candidate for future multiple-antenna aided systems, where estimating all the links may become unrealistic, especially in high-speed environments. Upon exploiting the correlation between the phase distortions experienced by the consecutively transmitted symbols and/or based on mutually and iteratively utilizing the increasingly improved bit reliability information among the associated multiple symbols in the context of differentially modulated systems using channel code aided iterative receivers, the joint processing on consecutively received multiple symbols improves the system's performance. For example, an increased robustness against rapid channel fluctuation, improved flexibility in the system's performance-complexity compromise as well as a reduced performance loss is achieved in comparison to its coherent detection aided counterpart. In order to stimulate further research on differentially modulated systems and on the associated multiple-symbol signal processing based advanced receiver design, a comprehensive review on their related concepts and fundamental principles is carried out in this treatise, followed by a number of potential challenges encountered in their practical implementations in future high-spectral-efficiency wireless transmissions, such as their applications in high-order differentially modulated systems and in differential interference suppression of spatial-division multiplexing/multiple access scenarios.**

***Index Terms*—Multiple-symbol detection, non-coherent detection, cooperative communications, sphere detection.**

I. Introduction

THE MAIN driving force behind the advances in wireless communications over hostile, band-limited radio channels is the promise of mobile multimedia communication with seamless global mobility and ubiquitous accessibility. A typical system of this kind is the mobile Internet, where information exchanges are supported among people and/or devices, regardless of their geographic positions, using different media within the same radio link, such as video, graphics, speech, text or other data. This implies that a mobile multimedia communication system has to adapt itself to the very different requirements of the individual services in terms of data rates, quality of service (QoS), maximum delay, etc. Therefore, against the backcloth of the explosive expansion of the Internet and the continued dramatic increase in demand for high-data-rate high-mobile-velocity multimedia services, it is increasingly important to find both energy- and bandwidth-efficient solutions for next-generation wireless communication, which is capable of coping with the associated severely frequency- and time-selective wireless channels.

In the context of traditional single-carrier wireless communication systems using coherent detection techniques, the above-mentioned propagation conditions encountered by high-data-rate and high-velocity applications are directly translated to significant increases in the equalization complexity as well as in channel estimation overheads. Although technological advances in integrated circuits and radio-frequency electronics facilitate the employment of ever more sophisticated signal processing and coding algorithms, a key consideration for the development of next-generation wireless communication systems is the support of small, low-cost user equipment (UE) with long battery life, both in stand-by and during activity. Thanks to its low-complexity discrete Fourier transform (DFT) based implementation, the orthogonal frequency-division multiplexing (OFDM) technique [1] and its variants[1] have become the predominant wideband transmission techniques. Their main benefit is that they facilitate low-complexity single-tap multiplicative equalization at the receiver.

As an important further invention, the innovative concept of Spatial Multiplexing (SM) invoked for increasing the throughput of wireless systems using multiple transmit and receive antennas (MIMO) was patented in 1994 [2]. This concept was inspired by carefully evaluating the signal separation experiments carried out by Paulraj and Kailath [2]. In the late 90s, as the integrated circuits and radio-frequency electronics have advanced in parallel to the increasing tele-traffic demands,

Manuscript received October 8, 2012; revised April 20, 2013. The research leading to these results has received funding from the European Union's Seventh Framework Programme ([FP7/2007-2013]) under grant agreement no [214625]. The financial support of the RC UK under the auspices of the UK-India Advanced Technology Centre of Wireless Communications and of the China-UK Science Bridge in 4G wireless communications, as well as that of the EU's Concerto project is also gratefully acknowledged.

The authors are with the School of ECS, University of Southampton, SO17 1BJ, U.K. (e-mail: lw5@ecs.soton.ac.uk; lh@ecs.soton.ac.uk).

Digital Object Identifier 10.1109/SURV.2013.081313.00218

[1]For example, orthogonal frequency-division multiple access (OFDMA), wideband code-division multiple access (WCDMA) and single-carrier frequency-division multiple access (SC-FDMA) are broadband transmission techniques developed based on the fundamental OFDM principle.

the research of MIMO systems was further fuelled by the pioneering work of Foschini [3, 4] and Telatar [5]. The fundamental philosophy was centered around efficient *space-time* signal processing [6–10]. As a substantial benefit, the family of MIMO techniques exhibits a capacity, which is linearly dependent on the minimum of the number of transmit and receive antennas [3, 11, 12]. Hence their throughput increases linearly with the number of MIMO elements and the transmit power. On the other hand, the benefits of MIMO systems may also be exploited for mitigating the detrimental effects of multipath propagation with the aid of their transmit/recieve diversity gain, which is an explicit benefit of receiving multiple independently faded transmit signal replicas [6, 7, 10]. Following years of intensive research, MIMO techniques have found their way into the wireless standards and hence they constitute one of the most significant technical inventions in contemporary wireless communications [13, 14]. More explicitly, they have reached commercial maturity and hence they are employed in wireless products and networks, such as broadband wireless access systems, wireless local networks (WLAN), third generation networks and in the most recent 3GPP LTE/LTE-Advanced networks.

However, it is typically impractical for the pocket-sized mobile device to employ multiple antennas due to its size and cost constraints as well as owing to the associated hardware impairments[2]. In addition, owing to the limited separation of the antenna elements, the transmitted signal rarely experiences independent fading, which in turn erodes the achievable diversity gain. The diversity gain may be further compromised by the deleterious effects of the large-scale shadow fading [15], since all the MIMO channels tend to fade together rather than independently, imposing further signal correlation amongst the antennas in each other's vicinity. Apart from the above obstacles in the way of achieving multiple-antenna-aided diversity gains, wireless cellular networks aim for improving the coverage, capacity or the quality of end-user experience (QoE) in inadequately covered areas, such as for example indoor environments and rural areas. The dense deployment of fully-fledged base stations (BSs) constitutes a high-quality solution, albeit this may impose a high infrastructure cost and thus may become economically unavailable, especially in low-traffic-density sparsely populated rural areas.

Hence, to meet the above challenging requirements of next-generation wireless networks, the family of relay-aided cooperative transmission technique [16–20] appears to be one of the most promising solutions. In a nutshell, in multi-user wireless systems, single-antenna-assisted mobile stations (MS) may cooperatively share their antennas in order to achieve the so-called cooperative diversity as well as a path-loss-reduction based power gain by forming a virtual antenna array (VAA) [21, 22] in both uplink (UL) and downlink (DL) transmissions. The concept of user cooperation has been first proposed in [19, 20] for a two-user cooperative CDMA system, where orthogonal codes are employed by the active users in order to avoid the multiple access interference. Naturally, the extra tele-traffic between a source MS and a cooperating MS serving as a relay station (RS) requires additional radio resources to be allocated - any of the well-established multiple access schemes can be employed by the users to guarantee their orthogonal interference-free transmission, such as time-division multiple access (TDMA), frequency-division multiple access (FDMA) or code-division multiple access (CDMA) [17].

According to the operations carried out at the RS, the relaying protocols may be classified into three categories, namely amplify-and-forward (AF), decode-and-forward (DF) and compress-and-forward (CF) relaying. In the AF scheme, which is also referred to as the analog-repeater-based arrangement [18], the RS simply amplifies and forwards the source node's 'overheard' signal to the intended destination, thus potentially increasing the system's overall noise level, since the signal and noise are amplified together. As to the DF scheme, the RS fully decodes the signal received from the source and provides the destination with a re-encoded signal. Hence, the problem of error propagation may arise, when the RS forwards the erroneously recovered signal, which may deteriorate the detection at the destination and hence the overall system performance. Recently, the CF-based cooperative scheme also received increasing research attention [23, 24], where the RS forwards a quantized or compressed version of the signal received from the source.

A. Notations Used in this Treatise

Before continuing our discourse, let us first detail the notations that we will shortly encounter in later sections. We generally use boldface variables to denote matrices as well as vectors. Furthermore, v_m is the mth element of the vector $\mathbf{v}$, while $M_{i,j}$ denotes the element located in the ith row and jth column of the matrix $\mathbf{M}$. Similarly, we use $\mathbf{M}_{i:j,m:n}$ to represent a $(j-i+1)\times(n-m+1)$-dimension submatrix of the matrix $\mathbf{M}$ spanning the region extended from the ith to the jth row and from the mth to the nth column. A block matrix $\underline{\mathbf{M}}$ is defined by vertically concatenating a number of matrices. Moreover, $\mathbf{M}^{\mathrm{d}} = \mathrm{diag}\{\mathbf{m}\}$ represents that the diagonal matrix $\mathbf{M}^{\mathrm{d}}$ is constructed by aligning the elements of the vector $\mathbf{m}$ along its diagonal. Likewise, we can define the block-wise diagonalization operation as: $\underline{\mathbf{M}}^{\mathrm{d}} = \mathrm{diag}\{\underline{\mathbf{M}}\}$, where the vertically concatenated element submatrices of block matrix $\underline{\mathbf{M}}$ is aligned along the diagonal of the block diagonal $\underline{\mathbf{M}}^{\mathrm{d}}$. Conventially, $\det(\mathbf{S})$ and $\mathbf{S}^{-1}$ are the determinant and inverse of a square matrix $\mathbf{S}$, respectively. For any general matrix $\mathbf{M}$, $\mathbf{M}^{\mathrm{H}}$ represents the conjugate transpose. Finally, $E\{\cdot\}$ means expectation.

B. Motivation Behind Differentially Encoded Wireless Communications

It is noteworthy that the substantial benefits promised by the above-mentioned multiple-antenna-based non-cooperative and cooperative MIMO systems may only be realized under the assumption of sufficiently accurate channel estimation, which however is likely to become a significantly more challenging issue than in the conventional single-input single-output (SISO) scenario. To be specific, the estimation of MIMO channels imposes an exponentially increased complexity with

[2]For example, the associated mixed-signal coupling and cross-talk that may become critical in integrated high performance wireless systems, where the digital circuitry is tightly co-located with the analog RF electronics.

the number of antennas. This will become more explicit, if we consider the simple example of an (8×8)-element MIMO system, where the estimation of a total of 64 propagation links between one pair of transceiver is required! Moreover, as mentioned previously, since future wireless communications will have to support a high grade of mobility[3] [25, 26], the relative frequency of estimating the channel has to be increased proportionately to the channel's fluctuation rate characterized by the Doppler frequency. Since the knowledge of channel state information (CSI) is typically obtained using a channel sounding sequence in practice[4], a substantially increased pilot-overhead is also expected, leading to a potentially significant reduction in both bandwidth and power efficiency.

Furthermore, performance degradations may occur when the receiver has imperfect CSI, as illustrated by the BER curve of a (2×1)-element G_2-aided MIMO system [6] in Fig. 1, where we assume that the channel estimation errors obey the Gaussian distribution and the degree of the CSI estimation errors is governed by the ratio ω (dB) with respect to the received signal power. Hence, the perfect CSI scenario corresponds to $\omega = -\infty$. To be specific, given a target BER of 10^{-5}, a performance loss of 5 dB may be encountered, even when the channel estimation errors are as low as $\omega = -24$ dB. Furthermore, when this second-order transmit diversity achieved by the G_2 scheme is attained with the aid of a VAA in the context of a single-relay-aided cooperative system, the achievable BER performance may become even more sensitive to the imperfect channel knowledge, as also evidenced in Fig. 1. Observe in Fig. 1 that even when the channel estimation errors are as low as -26 dB, the BER curve of the single-relay-aided AF system tends to exhibit an error floor above 10^{-5}. Thus the second-order transmit diversity originally achieved in the presence of perfect channel knowledge vanishes. This is because the cooperative system requires the CSI knowledge of both the source-to-relay and relay-to-destination links in comparison to the classic single-phase direct transmission regime of non-cooperative MIMO systems [28, 29]. By contrast, it is particularly challenging for the destination to accurately estimate the source-relay channel using pilot signal forwarding in the context of AF-based cooperative systems, since the pilots may be further contaminated by relay-induced noise amplification. Based on our above discussions, obtaining sufficiently accurate CSI for MIMO systems, particularly for the family of cooperative systems, may potentially impose both an excessive complexity and a high pilot overhead, especially when the number of antennas/cooperating users is high and/or when the channel conditions fluctuate relatively rapidly in high-velocity mobile environments.

Therefore, differentially encoded signaling combined with low-complexity non-coherent detection [30] and thus bypassing the complex yet potentially inaccurate channel estimation process at the receiver becomes an attractive design alternative, whose applications in MIMO systems has attracted considerable attention in the last decade, especially in cooperative communications [31–39].

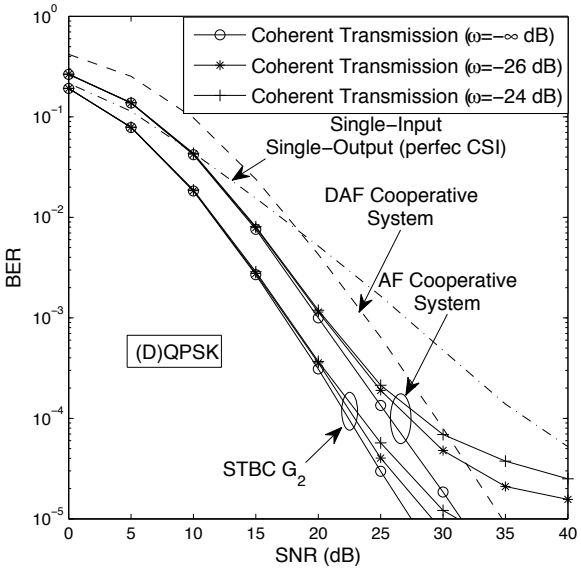

Figure 1. Performance sensitivity to imperfect channel knowledge of the single-relay amplify-and-forward TDMA cooperative system in conjunction with coherent detection.

C. Focus and Outline of the Paper

In view of the benefits of by-passing the potentially excessive-complexity and yet inaccurate channel estimation, the family of differential modulation schemes combined with non-coherent detection is advocated in this treatise as a viable candidate to be employed in the context of multiple-antenna-assisted systems, particularly for VAA-based cooperative systems. Nonetheless, as we will reveal in our forthcoming introduction of the conventional differential detection (CDD) scheme in Section II, CDD has its own limitations. For example, it is sensitive to rapid channel fluctuations owing to the radically faded reference symbols, which leads to a potential error-floor. Furthermore, typically exhibits a 3-dB performance loss in comparison to its coherent detection aided counterpart, which is due to the fact that in the presence of any channel-induced errors the next symbol also becomes erroneous owing to using an erroneous reference symbol. Hence substantial further research is required for designing advanced, improved-performance non-coherent receivers for mitigating the above-mentioned limitations of differentially encoded systems. Thanks to the recursive differential encoding procedure, joint processing of multiple successively received symbols constitutes a promising solution for significantly enhancing the performance of the conventional single-symbol signal processing based non-coherent receiver. The underlying philosophy behind the multiple-symbol joint signal processing is to exploit the correlation between the phase distortions experienced by the consecutively transmitted symbols and/or to mutually and iteratively exploit the increasingly improved

[3]The major candidates for the next generation of broadband wireless access systems, such as 3GPP-LTE and IEEE 802.16m, are expected to deliver a data rate of at least 100 Mbps for high-velocity mobile users (up to 350 km/h).

[4]Channel estimation can be realized by inserting so-called pilot symbols with known modulation into the transmitted signal. Based on these pilot symbols the receiver can measure the channel transfer factors (CTF) for each subcarrier in an OFDM system using interpolation techniques [27]. In this case, each subcarrier can be demodulated coherently.

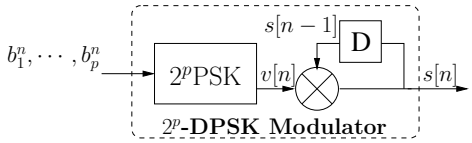

Figure 2. The schematics of 2^p-DPSK modulator.

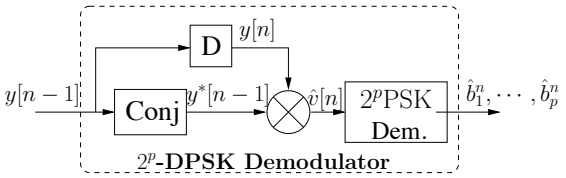

Figure 3. The schematics of 2^p-DPSK demodulator.

bit reliability information of the associated multiple symbols in the context of a channel code aided iterative receiver.

Against this backdrop, our goal is to stimulate further research on differentially encoded wireless systems. Hence we identify and address a number of fundamental challenges encountered in their maximum-a-posteriori (MAP) multiple-symbol joint signal processing based advanced receiver design. We will consider a variety of application scenarios and further develop the sphere detection (SD) mechanism for the sake of achieving a substantial complexity reduction, as detailed below:

- Differential amplitude and phase shift keying (DAPSK) [40, 41] - also known as Star Quadrature Amplitude Modulation (Star-QAM) - constitutes an attractive design alternative for high-data-rate differentially encoded transmissions. The decision-feedback differential detection (DF-DD) principle has been successfully applied to DAPSK systems in [42] as a low-complexity solution. This is complexity reduction is achieved at a modest, but non-negligible performance loss in comparison to the optimum maximum-likelihood multiple-symbol differential detection (ML-MSDD) owing to the potential feedback error propagation. Thus, designing a low-complexity near-optimum differential detector is beneficial.
- An efficient implementation of the MSDD specifically designed for the high-data-rate differential unitary space-time modulation (DUSTM) using the non-constant-modulus QAM constellation - rather than the conventional constant-modulus PSK constellation - constitutes another challenging problem to solve.
- For the sake of further improving the spectral efficiency, spatial-domain co-channel interference suppression scheme has been proposed for multiple-antenna-assisted differentially encoded wireless systems by taking advantage of the recursive nature of the differential encoding mechanism. In order to enhance the system's robustness against hostile wireless channels, the multiple-symbol joint processing regime may be further developed to amalgamate both interference filtering and signal detection, which is a challenging, but worthwhile issue to tackle.

To this end, we commence by reviewing the fundamental principle of the conventional differential encoding and decoding process in Section II. Then, following the construction of the generalized multiple-symbol system models for both co-located and distributed/cooperative MIMO systems in Section III-A, the principle of the maximum-likelihood-based MSDD (ML-MSDD) and that of its SD-based version, namely the MSDSD, is reviewed in Section III-B. Subsequently, the challenging design of MSDSD for non-constant-modulus modulation assisted bandwidth-efficient orthogonal SISO and MIMO systems is discussed in Sections IV-A and IV-B, respectively. Then, we move on to another promising mechanism capable of achieving a high bandwidth-efficiency for nonorthogonal transmission relying on spatial-domain interference mitigation and its multiple-symbol filtering as well as detector design in Section V. Finally, our concluding remarks are provided in Section VI.

II. Differential Encoding and Decoding

A. Fundamental Principles

Let us now consider the classic differential phase shift keying (DPSK) scheme for the single-transmit-antenna scenario, as portrayed in Fig. 2. In order to avoid channel estimation at the receiver, the transmitter differentially encodes its PSK-modulated information symbols $v[n] \in \mathcal{M}_c = \{e^{j2\pi m/2^p}; m = 0, 1, \cdots, 2^p - 1\}$ as $s[n] = s[n-1]v[n]$, where $v[n]$ contains the p-bit information $[b_1^n, b_2^n, \cdots, b_p^n]$. Essentially, the information is encoded as the phase difference between consecutively transmitted symbols, as shown in Fig. 2. At the receiver the corresponding conventional differential detector (CDD) [30], as depicted in Fig 3, may extract the data by simply calculating the phase difference between successive time samples without any CSI knowledge, under the assumption of slow channel-fluctuation. When the extra spatial dimension becomes available, which is an explicit benefit of having multiple antennas at both the transmitter and the receiver, the information can be differentially encoded using the previous symbols as reference in both the spatial and temporal dimensions, instead of using only the classic differentially encoded time-domain modulation scheme of Fig. 2. This leads to the differential space-time modulation (DSTM) aided transmission philosophy of $\mathbf{S}[n] = \mathbf{S}[n-1]\mathbf{V}[n]$ [43, 44]. This philosophy is shown in Fig. 4, where $\mathbf{S}[n]$ and $\mathbf{V}[n]$ are typically unitary matrices representing the differentially encoded space-time signal and the space-time information signal, respectively. Readers who are interested in more details on DSTM are referred to the citations seen in Tables I and II, as well as to the references therein. Naturally, in the light of the distributed space-time coding principles, the differential space-time coding regime can also be implemented in a distributed manner for user-cooperation aided systems [45–48].

B. Inherent 3 dB Performance Loss

Since the CDD recovers the information by directly calculating the phase difference of the two consecutively received symbols, it is intuitive that in the CDD-aided system, any received symbol that has been heavily noise-contaminated is likely to cause errors in recovering a pair of the consecutively differentially encoded information symbols. In other words,

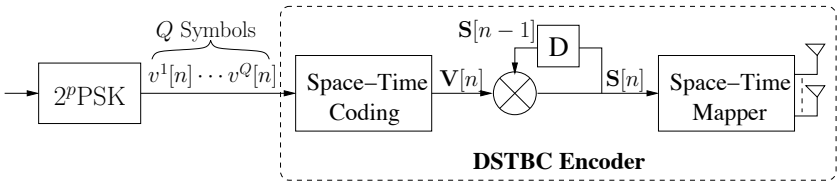

Figure 4. Schematic of a co-located MIMO system equipped $N_{\rm t}$ transmit and $N_{\rm r}$ receive antennas employs DUSTM, while transmitting Q symbols over T time slots using a differentially encoded space-time matrix $\mathbf{S}[n]$.

Table I
MAJOR CONTRIBUTIONS ADDRESSING THE DESIGN OF DUSTM FOR NON-COOPERATIVE MIMO SYSTEMS.

Author(s)	Contribution
[49] Tarokh *et. al.* 2000	Proposed the differential version of Alamouti's scheme [6].
[43] Hochwald *et. al.* 2000 [44] Hughes 2000	Introduced the family of differential unitary space-time modulation (DUSTM).
[50] Shokrollahi *et. al.* 2001	Proposed to design DUSTM using the theory of fixed-point free groups and their representations.
[51] Hassibi *et. al.* 2002	Designed DUSTM based on the Cayley transform.
[52] Zheng and Tse 2003	Derived the capacity of non-coherent MIMO channels.
[53] Nam *et. al.* 2004	Extended the work of [49] to four antennas.
[54] Zhu *et. al.* 2005	Designed DUSTM using the quasi-orthogonal philosophy.
[55] Oggier 2007	Proposed to design DUSTM based on cyclic algebra [56].

Table II
MAJOR CONTRIBUTIONS ADDRESSING THE DESIGN OF DUSTM FOR DISTRIBUTED MIMO SYSTEMS.

Author(s)	Contribution
[57] Wang *et. al.* 2006	Proposed DSTBC for AF relaying and its power allocation scheme.
[58] Yiu *et. al.* 2006	Proposed DSTBC using a unique node signature vector for DF relaying.
[59] Jing and Hamid 2008	Proposed distributed DSTBC for any relay numbers via circulant matrices.
[60] Rajan *et. al.* 2008	Designed distributed DSTBC using the extended Clifford algebras.
[61] Oggier *et. al.* 2009	Design distributed DSTM based on Cayley codes for any relay numbers.
[62] Gao *et. al.* 2011	Design DSTM for multi-source cooperation based on network coding.
[63] Huo *et. al.* 2012	Designed distributed DSTM for two-way relay using analog network coding.

the differentially modulated transmission detected by the CDD scheme circumvents the channel estimation at the expense of doubling the equivalent noise power, which in turn leads to a 3 dB performance loss in comparison to its coherent-detection-aided counterpart assuming perfect CSI knowledge, as indicated by the gap between the BER curves associated with the single-relay AF and differential AF (DAF) TDMA cooperative systems in Fig. 1. However, this coarse comparison between the coherent and non-coherent detection based systems seems to be unfair, since the perfect channel estimation is simply assumed for the coherent detection assisted system without taking the indispensable pilot overhead into account. For instance, if the avoidance of periodic transmission of pilot symbols can be exchanged for the adoption of a lower coding rate channel coding in the non-coherent system, the above-mentioned performance loss is in all fairness actually lower than what it seems to be, let alone the detrimental impact of an imperfect CSI knowledge on the coherent detection based system. Please refer to [64] for more comprehensive comparative studies between the relevant non-coherent and pilot-based coherent schemes. In order to mitigate the associated performance loss, the ML-MSDD scheme exploits the correlation between the phase distortions experienced by the consecutively transmitted symbols, as detailed in the forthcoming Section III.

C. Effects of Channel Fluctuations on Differential Decoding

According to the differential encoding mechanism illustrated in Fig. 2, the nth information symbol $v[n]$, which is encoded as the phase difference between the corresponding consecutively transmitted symbols $s[n-1]$ and $s[n]$, may not be recovered by the CDD process, if the two successively transmitted symbols experience quite different phase distortions caused by the rapid fluctuations of the fading coefficient in high-velocity mobile environments, even in the absence of noise. Similar high-Doppler-induced impairments may also occur in pilot-assisted coherent detection based transmissions. More explicitly, owing to the channel-induced noise-contamination of pilots, it is insufficient to sample the channel's frequency-domain transfer function at its Nyquist-frequency. Hence typically an over-sampling is used, thus imposing an increased pilot overhead. As a simple example, which quantitatively shows the detrimental effects of the channel's fluctuation on the performance of CDD, we consider here a DQPSK modulated uncoded OFDM system employing a sufficiently long cyclic prefix length. Hence we assume that no inter-OFDM-symbol interference is imposed. We assume furthermore that differential encoding is carried out along the time direction, i.e. between the same subcarriers of consecutive OFDM symbols[5]. Since a temporally Rayleigh-distributed fading is assumed for each subcarrier employed by the OFDM system, where the fading coefficients are correlated as a function of the time, the temporal autocorrelation function of the frequency domain channel transfer function (FD-CTF) h may be expressed as:

$$\varphi_{hh}[\kappa] \triangleq \mathcal{E}\{h[n+\kappa]h^*[n]\} = J_0(2\pi f_d \kappa), \qquad (1)$$

where $J_0(\cdot)$ denotes the zero-order Bessel function of the first kind and f_d is the normalized Doppler frequency. Figure 5(a)

[5]Similar results may be obtained if the differential encoding is conducted along the frequency direction, i.e. among adjacent subcarriers of a given OFDM symbol. The channel fluctuation rate in the frequency direction is a function of the maximum delay spread.

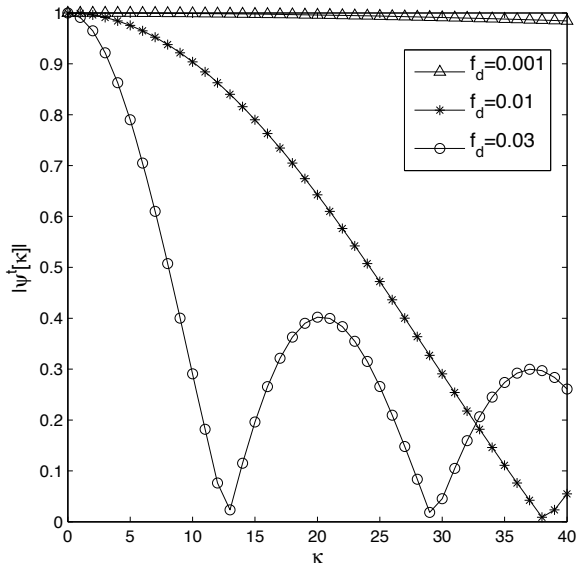

(a) Magnitude of temporal correlation function of Rayleigh fading channels

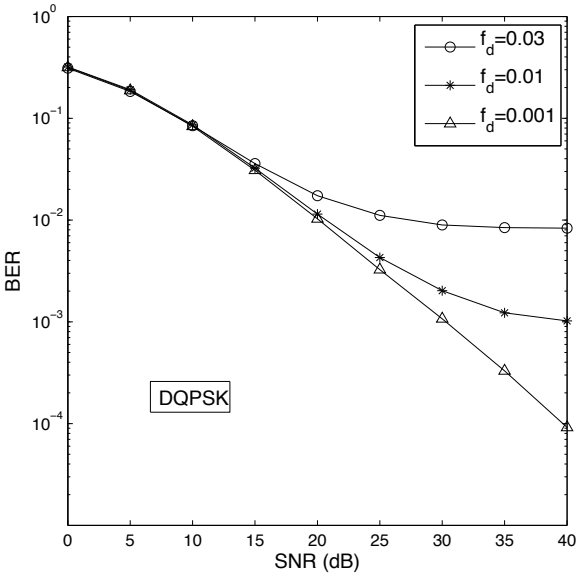

(b) Effects of dopper frequency on performance of CDD

Figure 5. Impact of mobility on the performance of CDD.

depicts the magnitude of temporal correlation function for various normalized Doppler frequencies f_d, while Figure 5(b) plots the corresponding BER curves of the DQPSK modulated CDD-aided OFDM system. It is observed that the BER curve tends to create an error floor, when f_d becomes high, which is caused by the high grade of relative mobility between the transmitter and the receiver.

III. Multiple-Symbol Differential Detection for Generalized MIMO Systems

A. Generalized Multiple-Symbol Reception Models

1) Co-Located MIMO System: In the context of the MIMO-OFDM system, non-dispersive fading is encountered by each sub-carrier, provided that the number of sub-carriers is sufficiently high. Since the differential encoding is assumed to be conducted along the time-domain for each frequency domain (FD) sub-carrier throughout this treatise unless otherwise stated, the multiple-symbol signal processing mechanisms discussed in the ensuing sections may be carried out on a per-sub-carrier basis at the receiver, which are thus equally applicable to the single-carrier narrowband modems. Hence, let us consider the following per-sub-carrier-based FD system model constructed for multiuser OFDM systems supporting U differential-modulation-based $N_{\rm t}$-antenna-aided uplink (UL) MSs with the aid of $N_{\rm r}$ receiver antennas at the BS [1]. We assume that orthogonal interference-free transmission amongst the U MSs is guaranteed by means of the conventional multiple access schemes, such as for example TDMA, thus the *single-symbol* transmission model constructed for the uth MS and corresponding to the nth space-time signal's transmission can be formulated as[6]:

$$\mathbf{Y}[n] = \mathbf{S}[n]\mathbf{H}[n] + \mathbf{W}[n], \tag{2}$$

where $\mathbf{Y}[n] \in \mathbb{C}^{N_{\rm t}\times N_{\rm r}}$, $\mathbf{S}[n] \in \mathbb{C}^{N_{\rm t}\times N_{\rm t}}$ and $\mathbf{W}[n] \in \mathbb{C}^{N_{\rm t}\times N_{\rm r}}$ denote the FD received and transmitted space-time signal matrices as well as the AWGN matrix having a distribution of $\mathcal{CN}(0, 2\sigma_w^2 N_{\rm r}\mathbf{I}_{N_{\rm t}})$, respectively. Each $N_{\rm t}$-antenna-aided MS first generates the space-time information signal $\mathbf{V}[n]$, which is then differentially encoded as $\mathbf{S}[n] = \mathbf{V}[n]\mathbf{S}[n-1]$, where the rows and columns of $\mathbf{S}[n]$ denote the time and space dimensions, respectively. Furthermore, the FD-CTF matrix $\mathbf{H}[n]$ is a $(N_{\rm t} \times N_{\rm r})$-dimensional i.i.d. zero-mean unit-variance complex Gaussian matrix, which is assumed to remain unchanged within the nth space-time signal duration, i.e. $N_{\rm t}$ time slots. Thanks to the differential encoding process at the MS, the knowledge of the FD-CTF matrix $\mathbf{H}[n]$ is not required for recovering the transmitted information $\mathbf{V}[n]$ at either the MS or the BS of the MIMO-OFDM system considered. For instance, the CDD decision rule $\hat{\mathbf{V}}[n] = \arg\min_{\check{\mathbf{V}}[n]}\{||\mathbf{Y}[n] - \check{\mathbf{V}}[n]\mathbf{Y}[n-1]||^2\}$ may be invoked, which is capable of achieving a reasonably good performance in a slow-fading channel where we have $\mathbf{H}[n-1] \approx \mathbf{H}[n]$.

On the basis of the single-symbol system model of (2) we now construct the per-sub-carrier-based *multiple-symbol* MIMO-OFDM system model as:

$$\underline{\mathbf{Y}}[k_N] = \underline{\mathbf{S}}^{\rm d}[k_N]\underline{\mathbf{H}}[k_N] + \underline{\mathbf{W}}[k_N], \tag{3}$$

where the block matrix index k_N denotes the kth block matrix constituted of $N_{\rm wind}$ component matrices. For example, the kth received space-time signal block matrix $\underline{\mathbf{Y}}[k_N]$ of (3) contains $N_{\rm wind}$ consecutively received space-time signal matrices. Hence we have $\underline{\mathbf{Y}}[k_N] = [\mathbf{Y}[(N_{\rm wind}-1)(k-1)]^T \cdots \mathbf{Y}[(N_{\rm wind}-1)k]^T]^T$. Similarly, both the kth FD-CTF block matrix $\underline{\mathbf{H}}[k_N]$ as well as the AWGN's kth block matrix $\underline{\mathbf{W}}[k_N]$ are defined by vertically stacking the $N_{\rm wind}$ matrices $\mathbf{H}[n]$ and $\mathbf{W}[n]$ $(n = (N_{\rm wind}-1)(k-1), \cdots, (N_{\rm wind}-1)k)$ of (2), respectively. Moreover, the kth diagonal block matrix of the transmitted signal $\underline{\mathbf{S}}^{\rm d}[k_N]$ of each MS is constructed as $\underline{\mathbf{S}}^{\rm d}[k_N] = {\rm diag}\{\underline{\mathbf{S}}[k_N]\} = {\rm diag}\{[\mathbf{S}[(N_{\rm wind}-1)(k-$

[6]Both the user and sub-carrier indices are omitted here for notational simplicity.

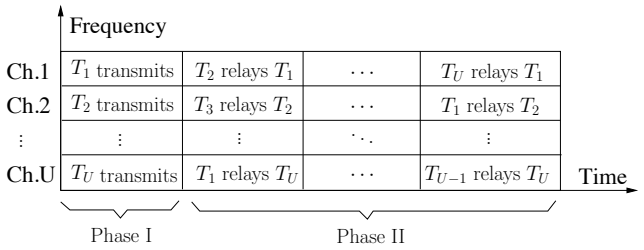

Figure 6. Channel allocation scheme for the cooperative cluster formed by U MSs in a celluar UL system.

$1)]^{\mathrm{T}} \ \cdots \ \mathbf{S}[(N_{\mathrm{wind}}-1)k]^{\mathrm{T}}]^{\mathrm{T}}\}$, which corresponds to the length-$(N_{\mathrm{wind}}-1)$ space-time information signal block matrix $\underline{\mathbf{V}}[k_N] = [\mathbf{V}[(N_{\mathrm{wind}}-1)(k-1)+1]^T \ \cdots \ \mathbf{V}[(N_{\mathrm{wind}}-1)k]^T]^T$.

It is worth emphasizing that both the single-symbol and multiple-symbol MIMO-OFDM system models of (2) and (3) subsume the single-antenna-based SISO-OFDM system as a special case by setting $N_{\mathrm{t}} = N_{\mathrm{r}} = 1$.

2) Distributed MIMO System: Due to pratical cost and size constraints, the employment of multiple transmit antennas by each MS is typically infeasible. Fortunately, the cooperative sharing of antennas amongst MSs in multi-user scenarios constitutes a promising solution in order to achieve both cooperative diversity as well as a path-loss-reduction based power gain, as discussed in Section I. The often-used two-hop relay-aided systems will be considered in this section, which may be readily extended to more sophisticated cooperative systems. Moreover, only the AF and DF relaying stratages will be considered in this treatise, since they have become the most popular ones, thanks to their simplicity and intuitive designs.

As an example of the channel allocation depicted in Fig. 6 for the two-hop-relaying-based cooperative cluster formed by U MSs in a cellular UL system, the signal transmission involves two transmission phases owing to the half-duplex communications of practical transceivers, namely the broadcast phase and the relay phase. These are also often referred to as phase I and II. For the sake of simplicity, both TDMA as well as FDMA are considered, as illustrated in Fig. 6, in order to guarantee orthogonal, i.e. non-interfering transmission amongst cooperating MSs. Furthermore, since the channel allocation employed among cooperative users may be deemed to be symmetric, as indicated in Fig. 6, we now focus our attention on the information transmission of a specific MS (e.g. T_1) in the cellular UL scenario of Fig. 7. The MS T_1 may be assisted by $M_r = (U-1)$ RSs activated from the set of available cooperating MS candidate pool. Consequently, upon using the TDMA scheme of Fig. 6, the $M_r = (U-1)$ activated RSs of Fig. 7 successively process and forward the signal broadcast from the source MS to the BS.

For the differential DF (DDF) system, under the assumption of accurate signal recovery at each RS[7], an entire *single-symbol*-based cooperative transmission cycle of a specific source MS may be mathematically described in a form identical to (2) in co-located MIMO transmissions, albeit we have a different interpretation for each term therein. To be specific, when we employ (2) for describing the DDF system, we redefine $\mathbf{Y}[n] \in \mathbb{C}^{UN_{\mathrm{t}} \times N_{\mathrm{r}}}$, $\mathbf{S}[n] \in \mathbb{C}^{UN_{\mathrm{t}} \times UN_{\mathrm{t}}}$ and $\mathbf{W}[n] \in \mathbb{C}^{UN_{\mathrm{t}} \times N_{\mathrm{r}}}$ as the U-user-cooperation-based FD received and transmitted space-time signal matrices as well as the AWGN matrix having a distribution of $\mathcal{CN}(0, 2\sigma_w^2 N_{\mathrm{r}} \mathbf{I}_{N_{\mathrm{t}}})$, respectively. More specifically, since the classic TDMA-based mechanism is used during each cooperation cycle for a specific MS, $\mathbf{S}[n]$ is a diagonal block matrix with its top-left submatrix $\mathbf{S}[n]_{1:N_{\mathrm{t}},1:N_{\mathrm{t}}}$ denoting the space-time signal transmitted by the source MS and the diagonal submatrix $\mathbf{S}[n]_{mN_{\mathrm{t}}:(m+1)N_{\mathrm{t}},mN_{\mathrm{t}}:(m+1)N_{\mathrm{t}}}$ $(1 \le m \le U-1)$ being the space-time signal radiated by the mth RS. Accordingly, both the user-cooperation-based channel matrix $\mathbf{H}[n] \in \mathbb{C}^{UN_{\mathrm{t}} \times N_{\mathrm{r}}}$ and the AWGN matrix $\mathbf{W}[n]$ of (2) encapsulate the corresponding FD-CTF and additive noise between each cooperating MS and the BS, respectively, as illustrated in the single-antenna-based example (i.e. $N_{\mathrm{t}} = N_{\mathrm{r}} = 1$ as depicted in Fig. 7) of Table III. Note that a total power P is assumed to be shared by the collaborating MSs for transmitting a symbol. Thus, by assuming that M_r cooperating MSs are activated, we can express the associated power contraint as: $P = P_s + \sum_{m=1}^{M_r} P_{r_m}$, where P_s and P_{r_m} $(m = 1, 2, \cdots, M_r)$ are the transmit power employed by the source MS and the mth RS, respectively.

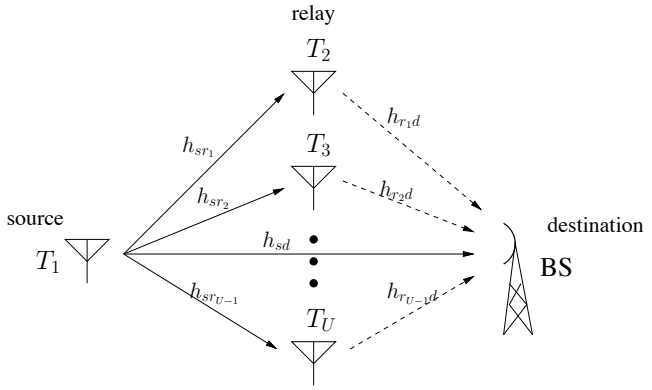

Figure 7. Schematic of a U-MS cooperative celluar UL system.

Similarly, in the context of the differential AF (DAF) cooperative system, the entire cooperative transmission cycle of a specific source MS may also be formulated in a form identical to (2). However, in contrast to the case of the DDF cooperative system, where the broadcast phase is actually excluded from (2) by invoking the perfect relaying assumption, the construction of (2) for the DAF cooperative system truly encapsulates a complete cycle of the cooperative transmission, including both the broadcast phase and the relaying phase. Specifically, the broadcast space-time signal matrix $\mathbf{S}[n]$ is a diagonal block matrix with its top-left submatrix $\mathbf{S}[n]_{1:N_{\mathrm{t}},1:N_{\mathrm{t}}}$ denoting the space-time signal transmitted from the source MS to the BS via the direct transmission path. The remaining diagonal sub-matrices $\mathbf{S}[n]_{mN_{\mathrm{t}}:(m+1)N_{\mathrm{t}},mN_{\mathrm{t}}:(m+1)N_{\mathrm{t}}} = \mathbf{S}[n]_{1:N_{\mathrm{t}},1:N_{\mathrm{t}}}$ $(1 \le m \le U-1)$ represent the space-time

[7]It was recently demonstrated in [21, 65] that the fixed DF system dispensing with any error-aware mechanisms at the RS, such as for example, the cyclic redundancy check [66], offers no diversity gain over its conventional direct-transmission-based counterpart. Hence, the selective DF scheme [21, 65] is assumed here with the aid of error detection codes and/or intelligent RS selection schemes, where only the RSs that correctly recover the source's signal may be activated in the the relay phase.

Table III
STRUCTURE OF $\mathbf{H}[n]$ AND $\mathbf{W}[n]$ OF (2) FOR BOTH THE DAF AND DDF SYSTEMS ($N_{\rm t} = N_{\rm r} = 1$ SEE FIG. 7)

	$\mathbf{H}[n] =$	$\mathbf{W}[n] =$
DDF System	$\left[\sqrt{P_s}h_{sd}[n],\ \sqrt{P_{r_1}}h_{r_1d}[n],\cdots,\ \sqrt{P_{r_{U-1}}}h_{r_{U-1}d}[n]\right]^{\rm T}$	$\left[w_{sd}[n],\ w_{r_1d}[n],\cdots,\ w_{r_{U-1}d}\right]^{\rm T}$
DAF System	$\Big[\sqrt{P_s}h_{sd}[n],\ \sqrt{P_s}f_{AM_{r_1}}h_{sr_1}[n]h_{r_1d}[n],$ $\cdots,\sqrt{P_s}f_{AM_{r_{U-1}}}h_{sr_{U-1}}[n]h_{r_{U-1}d}[n]\Big]^{\rm T}$	$\Big[w_{sd}[n],\ f_{AM_{r_1}}w_{sr_1}[n]h_{r_1d}[n]+w_{r_1d}[n],\cdots,$ $f_{AM_{r_{U-1}}}w_{sr_{U-1}}[n]h_{r_{U-1}d}[n]+w_{r_{U-1}d}[n]\Big]^{\rm T}$

signal transmitted from the source MS to the BS with the aid of the mth RS, which successively passes through the source-relay (SR) and relay-destination (RD) links. Again, for the sake of simplicity, in Table III we highlight the structure of the user-cooperation-based channel matrix $\mathbf{H}[n]$ and AWGN matrix $\mathbf{W}[n]$ in the context of the single-antenna-based (i.e. $N_{\rm t} = N_{\rm r} = 1$ as depicted in Fig. 7) DAF system. Note that $f_{AM_{r_m}}$ is the power amplification factor employed by the mth RS in order to ensure that the average transmit power of the mth RS becomes P_{r_m}, which is given in [67] as $f_{AM_{r_m}} = \sqrt{\frac{P_{r_m}}{P_s\sigma^2_{sr_m}+N_0}}$, with $\sigma^2_{sr_m}$ and $N_0 = 2\sigma^2_w$ being the variance of the channel's envelope between the source as well as the mth RS and the noise variance[8], respectively.

Therefore, based on the above discourse, we know that both the DAF and DDF cooperative systems may be mathematically described using the single-symbol system model in the form of (2). Furthermore, by employing the same approach of constructing the multiple-symbol system model from its single-symbol counterpart, as used for the co-located MIMO system in Section III-A1, it is now plausible that the multiple-symbol system models constructed for both the DAF and DDF cooperative systems obey the form of (3). In a nutshell, both the co-located and distributed MIMO systems considered may be formulated by the same mathematical model, which is advantageous for our non-coherent receiver design.

B. Multiple-Symbol Differential Detection

1) Principle of MSDD: It is worth emphasizing that all the elements in $\mathbf{H}[n]$ and $\mathbf{W}[n]$ exhibit a standard Gaussian distribution for all the systems discussed above, except for the DAF-based coopeartive system, where the relay-link-related components in $\mathbf{H}[n]$ and $\mathbf{W}[n]$ are products of two complex Gaussian variables, as we may observe from Table III. However, the detailed simulation-based investigations of [68] suggest that the resultant noise processes are near-Gaussian distributed. As a result, the PDF of the received signal vector $\underline{\mathbf{Y}}[k_N]$ in (3) recorded for the DAF cooperative system is also near-Gaussian, especially for relatively low SNRs, where the effects of the AWGN become more dominant. Hence, under the simplifying assumption that the *equivalent* fading and noise are zero-mean complex Gaussian processes, the PDF of the non-coherent receiver's output $\underline{\mathbf{Y}}[k_N]$ in (3) conditioned on the transmitted signal $\underline{\mathbf{S}}^{\rm d}[k_N]$ may be approximately expressed as follows for all the co-located and distributed MIMO scenarios considered[9]: $p(\underline{\mathbf{Y}}|\underline{\mathbf{S}}^{\rm d}) \approx \exp(-{\rm Tr}\{\underline{\mathbf{Y}}^{\rm H}\underline{\Psi}^{-1}\underline{\mathbf{Y}}\})/(\det(\pi\underline{\Psi}))^{N_r}$, where the conditional autocorrelation matrix is given by: $\underline{\Psi} = E\{\underline{\mathbf{Y}}\underline{\mathbf{Y}}^{\rm H}|\underline{\mathbf{S}}^{\rm d}\} = \underline{\mathbf{S}}^{\rm d}E\{\underline{\mathbf{H}}\underline{\mathbf{H}}^{\rm H}\}\underline{\mathbf{S}}^{\rm d^H} + E\{\underline{\mathbf{W}}\underline{\mathbf{W}}^{\rm H}\}$. The decision metric of the maximum-likelihood multiple-symbol differential detector (ML-MSDD) designed for the differentially encoded cooperative system may be expressed with the aid of Bayes' theorem as $\hat{\underline{\mathbf{V}}}^{\rm d}_{\rm ML} = \arg\min_{\tilde{\underline{\mathbf{V}}}^{\rm d}\in\mathcal{M}_c^{(N_{\rm wind}-1)}} {\rm Tr}\{\underline{\mathbf{Y}}^{\rm H}(\Psi)^{-1}\underline{\mathbf{Y}}\}$ [69], where $\mathcal{M}_c$ is the set of legitimate constellation points for $\mathbf{V}[n]$. Note that the choice of the first space-time signal of the current transmitted signal block contained in $\underline{\mathbf{S}}^{\rm d}$ serves as the reference signal, which does not affect the resultant ML solution. Therefore, the entire search space becomes $\mathcal{M}_c^{(N_{\rm wind}-1)}$ instead of $\mathcal{M}_c^{N_{\rm wind}}$. Consequently, the correlation between the phase distortions experienced by the consecutively transmitted symbols can be exploited by invoking the ML-MSDD decision metric, which is actually contained in the channel's covariance matrix $\Sigma_h = E\{\underline{\mathbf{H}}\underline{\mathbf{H}}^{\rm H}\}$. In practice, the channel's correlation matrix may be modelled by the well-known Jakes-model with the aid of the estimated Doppler frequency, namely relying on (1). According to [70], the predictability of the channel is characterized by the rank Q of the channel's covariance matrix Σ_h. For example, the block-fading channel, where the fading envelope remains constant over the entire fading block (i.e. k_N space-time signal durations), is associated with the most predictable fading envelope, when the channel's covariance matrix has a rank of $Q = 1$. By contrast, the fading process has a finite differential entropy and becomes less predictable, when we have $Q = k_N \cdot {\rm rows}(\mathbf{H}[n])$. Let us now consider the two-user-cooperation-based DAF UL system as a simple example for demonstrating the performance improvement achieved by the MSDD in a high-speed mobility environment, where two single-antenna-aided MSs cooperatively share their antennas to form a VAA. As observed in Fig. 8, upon using the CDD of Fig. 3 at the BS, the performance gain achieved by the DAF system over the traditional point-to-point direct transmission system erodes significantly, when the channel's fluctuation rate is high (e.g. associated with $f_d = 0.03$ in this case). Remarkably, the curve of Fig. 8 marked by circles suggests that the time-selective-fading-induced error floor may be substantially mitigated for the DAF system with the aid of MSDD by setting a sufficiently high window-length of $N_{\rm wind} = 6$. Naturally, when using the classic ML MSDD, the associated complexity becomes equivalent to $2^6 = 64$ objective function evaluations.

[8]The same noise variance is assumed at each receiver within the cooperative system throughout this treatise.

[9]In the interest of ease of presentation, the block index k_N is omitted here without loss of accuracy.

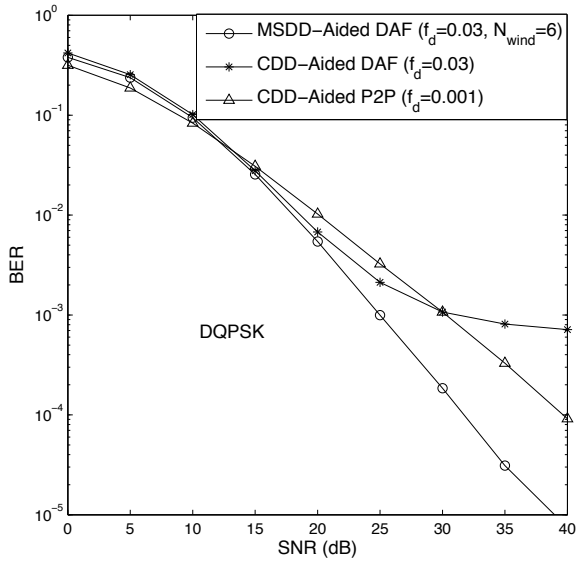

Figure 8. BER performance gain achieved by the MSDD for the single-relay-aided DAF system ($U = 2$, $N_{\rm t} = N_{\rm r} = 1$).

2) Complexity Reduction for MSDD: On the other hand, finding the ML-MSDD solution $\underline{\mathbf{S}}^{\rm d}_{\rm ML}$ is known to be NP-hard. Hence, a pontentially excessive computational complexity may be imposed, which is exponentially increased with both the constellation size M_c as well as the observation window size $N_{\rm wind}$ employed by the MSDD. Considering again the above DAF-based cooperative system for example, under the assumption of an observation window size of $N_{\rm wind} = 10$ and that of DQPSK ($M_c = 4$), $2^{20} = 1.048576 \times 10^6$ legitimate user-cooperation based space-time constellation points have to be evaluated, thus precluding the practical implementation of the ML-MSDD at the BS of our differentially encoded non-coherent cooperative system. As a remedy, the classic sphere decoding (SD) algorithm may be invoked, which was originally derived by Pohst and Finke [71] for efficiently calculating a vector of short length in a lattice. The SD was then further developed for coherent-detection-based communication systems [72] by Viterbo and Boutros. As a result, the coherent ML performance is approached at a moderate complexity, which is polynomially, rather than exponentially dependent on the number of unknowns. Inspired by above contributions, the SD algorithm was first introduced by Lampe *et al.* in [73] for mitigating the complexity of the ML-MSDD [74, 75] in the context of a differentially modulated SISO system, leading to the multiple-symbol differential sphere detection (MSDSD) concept. More recently, the employment of MSDSD is further extended to the family of co-located and distributed MIMO systems by Pauli and Lampe in [69] as well as by Wang and Hanzo in [68], respectively. Basically, the transplantation of the SD mechanism into the MSDD relies on the fact that $\underline{\mathbf{S}}^{\rm d}$ of (3) formed in the context of both the co-located and distributed MIMO systems considered is unitary, owing to the employment of conventional DPSK schemes or unitary space-time codes. After a few mathematical manipulations, which are omitted here in the interest of simplicity, the original ML-MSDD decision metric may be reformulated as $\hat{\underline{\mathbf{V}}}^{\rm d}_{\rm ML} = \arg\min_{\check{\underline{\mathbf{V}}}^{\rm d} \in \mathcal{M}_c^{(N_{\rm wind}-1)}} ||\underline{\mathbf{U}}\check{\underline{\mathbf{S}}}||^2 < R$, where $\check{\underline{\mathbf{V}}}^{\rm d} = {\rm diag}\{\check{\underline{\mathbf{V}}}\}$ and $\underline{\mathbf{U}}$ is an upper-triangular block matrix, which can be obtained as $\underline{\mathbf{U}} \triangleq (\mathbf{F} \otimes \mathbf{I}_{N_{\rm r}})({\rm diag}\{\underline{\mathbf{Y}}\})^{\rm H}$, with $\mathbf{F}$ also being an upper-triangular matrix generated using the well-known Cholesky factorization [76] of the matrix $(\Sigma_h + 2\sigma_w^2 \mathbf{I}_{N_{\rm wind}})^{-1}$. Consequently, thanks to the upper-triangular structure of the matrix $\underline{\mathbf{U}}$, a layered tree search may be carried out within a hyper-spheric search space, which is centered at the origin and confined by the SNR-dependent search radius R.

The MSDSD mechanism can be interpreted as a geometric problem, which is illustrated in Fig. 9. For the sake of simple visualization, we consider here a traditional point-to-point transmission system, which employs the DBPSK scheme at the transmitter and jointly detects $(N_{\rm wind} - 1 = 3)$ consecutively transmitted information symbols with the aid of the MSDSD scheme at the receiver upon observing the $(N_{\rm wind} = 4)$ successively received symbols. Thus, the corresponding multiple-symbol-based transmit domain constellation and the pertaining 3D search space in the receive domain is depicted in Fig. 9(a) and Fig. 9(b), respectively, in order to demonstrate how the SD mechanism works in the context of MSDD. At the receiver, the shape of the multiple-symbol-based cubic constellation of Fig. 9(a) is assumed to be distorted, due to the routinely encountered multipath induced phase rotation and magnitude attenuation. Instead of carrying out a full search in the receive domain over the entire candidate set of $(2^3 = 8)$ trial point, as the ML-MSDD would in order to find the optimum ML solution, the MSDSD initializes the search radius depending on the estimated SNR, which confines the search area to the outer-most sphere centered at the origin. As seen from Fig. 9(b), the search area is significantly reduced in comparison to that of the ML-MSDD scheme. It is indeed intuitive that only the trial lattice points residing in the immediate neighbourhood of the origin are worth examining. All the points in the search space confined by the radius are deemed to be tentative candidates for the three consecutively transmitted information symbols. Now the core operation of the MSDSD algorithm is activated. Specifically, a new radius is calculated by measuring the distance between a candidate randomly chosen within the spheric search space and the origin, which should be no higher than the original radius. Then another arbitrary multiple-symbol-based point is chosen from the newly obtained search space as the trial transmitted symbol. Again, the search radius is updated with the value of the distance between the newly obtained trial point and the origin. These operations are repeated, until the MSDSD finds that specific legitimate constellation point, which is nearest to the origin. At the end of the search, we assume that the last trial point that was found corresponds to the ML solution. In the example shown in Fig. 9(b), the MSDSD reaches the optimum ML solution after two radius updates. Hence, only three trial points are examined in terms of their Euclidean distance with respect to the origin. Therefore, the excessive-complexity full search carried out by the ML-MSDD is avoided by incorporating the SD mechanism into the MSDD scheme.

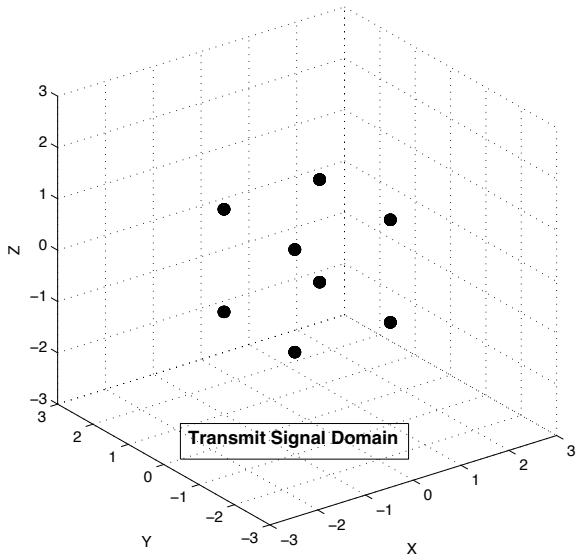

(a) Multiple-symbol-transmission-based transmit domain constellation.

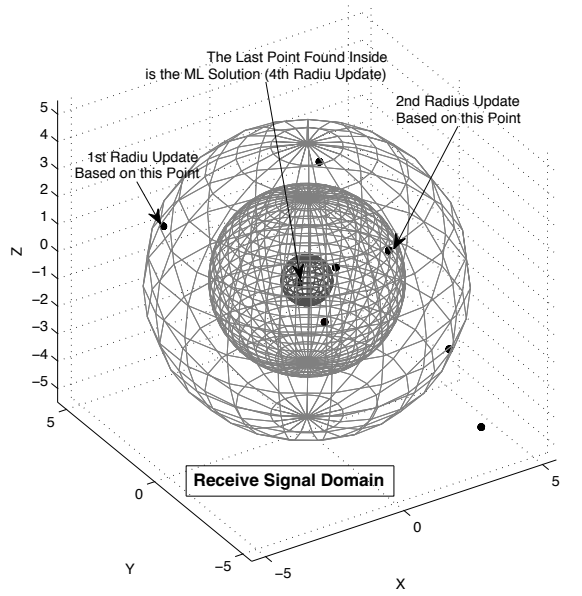

(b) MSDSD processing in the receive domain.

Figure 9. Geometrical interpretation of SD mechanism.

Another way of illustrating the SD algorithm's philosophy is constituted by the search tree example provided for the scenario of a DBPSK modulated system in conjunction with $N_{\text{wind}} = 5$ characterized in Fig. 10. As shown in Fig. 10, the depth-first SD commences its search procedure using an initial search radius of $R = 5$ from the top level $(n = 4)$. For each tree node, the number within the bracket denotes the corresponding accumulated partial Euclidean distance (PED) of that node from the origin, while the number outside the bracket indicates the order in which the node is visited. The broken line represents a binary zero, whereas the continuous

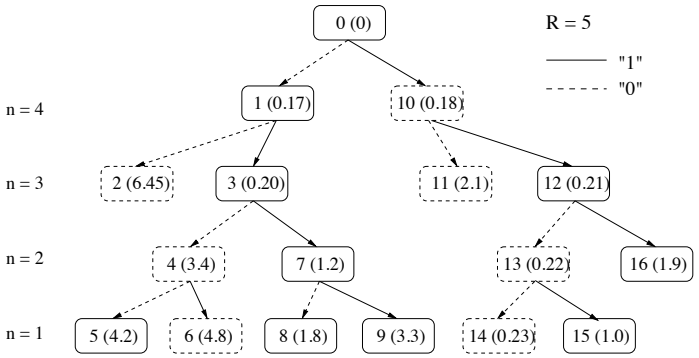

Figure 10. Illustration of the depth-first SD algorithm with the aid of the classic tree searching: The figure in ( ) indicates the partial Euclidean distance of a specific node for the trial point in the modulated constellation; while the number outside represents the order in which the points are visited. Finally, the ML solution of 1100 is found by choosing the tree leaf having the minimum Euclidean distance of 0.23 and backtracking to the level $n = 4$.

line denotes a binary one. As we can see in Fig. 10, the search is carried out from the left to the right, but in both downward and upward directions along the tree. Specifically, there are two scenarios that may be encountered during the tree search portrayed in Fig. 10. Firstly, the search may reach a leaf node at the bottom, i.e. level $(n = 1)$. The other possible scenario is that the detector cannot find any point inside the hyperspherical space for the nth element $\mathbf{V}[n]$, or equivalently, the accumulated PEDs of all the candidates for $\mathbf{V}[n]$ are higher than the current search radius R.

For example, in the first case, once the search reaches a leaf node, as seen at its fifth step, where the detector reaches a tree leaf having an Euclidean distance of 4.2 in Fig. 10, which is smaller than the current search radius of $R = 5$, then the detector starts the search process again with the reduced radius $R = 4.2$. In the second case, the detector must have made at least one erroneous tentative point selection for the previous $(N_{\text{wind}} - n - 1)$ lattice coordinates. In this scenario, the detector returns to the $(n+1)$th search tree level and selects another tentative point for $\mathbf{V}[n+1]$ within the hyperspherical space confined by the search radius. Following this, it proceeds downwards along the tree again to try and find a legitimate decision for $\mathbf{V}[n]$. If all the available tentative points for $\mathbf{V}[n+1]$ fail to lead to a legitimate decison, the search back-tracks to $\mathbf{V}[n+2]$ with the same objective, and so on. For example, at the ninth step seen in Fig. 10, the detector is unable to find a legitimate point within the new smaller hyper-sphere having the radius of 1.8, which was obtained at the previous step, hence the search back-tracks to level $n = 4$, since no more available candidates can be found within the corresponding search area for $\mathbf{V}[2]$, and $\mathbf{V}[3]$. In the end, after visiting a total of 15 tree nodes and leaves in Fig. 10, the SD chooses the specific tree leaf having a minimum Euclidean distance of 0.23 and back-tracks to the level $n = 4$ to generate the final ML solution of $\hat{\mathbf{V}}_{\text{ML}}$.

The interested reader is referred to [77–80] and the references therein for a more comprehensive treatment of the SD algorithms. Although our attention is focused on the MSDSD in this treatise, it is worth noting that a range mechanisms other than that of the SD scheme can also be employed for

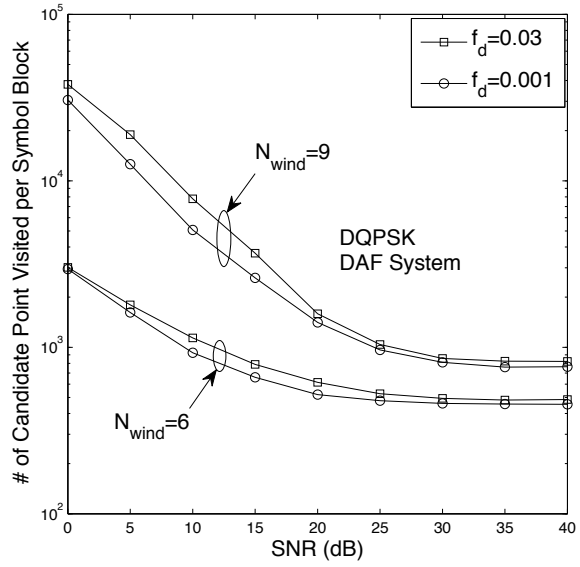

Figure 11. Complexity imposed by the MSDSD versus SNR in the single-relay-aided DAF system ($U = 2$, $N_{\rm t} = N_{\rm r} = 1$).

achieving a beneficial complexity reduction for the MSDD, such as those discussed in [81, 82].

The complexity quantified by the number of candidate block-symbol points $\underline{\check{\mathbf{S}}}$ enumerated during the tree search carried out by the MSDSD versus the SNR is plotted in Fig. 11 in the scenario of a DQPSK single-relay-aided DAF cooperative system. It is observed that the complexity imposed by the MSDSD is a function of the observation window size $N_{\rm wind}$, of the receive SNR as well as of the normalized Doppler frequency f_d. Specifically, as observed in Fig. 11, the complexity of MSDSD increases dramatically, once the original observation window size of $N_{\rm wind} = 6$ is set to $N_{\rm wind} = 9$. On the other hand, the complexity imposed by the MSDSD decreases only moderately, as the SNR increases and finally levels out in the high-SNR range. This is not unexpected, since under the assumption of having a reduced noise contamination, it is more likely that the ML solution point $\underline{\hat{\mathbf{S}}}^{\rm d}_{\rm ML}$ is located near the search center of the SD used for finding the ML-MSDD solution. As a result, the SD's search process may converge much more rapidly, imposing a reduced complexity. Furthermore, we can also observe from Fig. 11 that the Doppler frequency has a non-negligible effect on the complexity imposed by the MSDSD. Basically, for a constant value of $N_{\rm wind}$, a reduced grade of channel predictability associated with an increased Doppler frequency may lead to an increased complexity imposed by the MSDSD scheme.

IV. Design of MSDSD for High-Spectrum-Efficiency Differential Signaling Using Non-Constant-Modulus Constellations

Differential amplitude and phase shift keying (DAPSK) [40, 41, 83] using non-constant-modulus constellations was first proposed for digital terrestrial video broadcasting (DTVB) in [84, 85] in the context of a single-tranmsit-antenna-assisted systems employed in SISO or SIMO scenarios. Since broadcast receivers can be switched on at any moment in an asyncrhoneous manner, a high pilot-overhead would be necessary for a coherently detected system to facilitate near-isntantaneous reception. Furthermore, the coherent receivers are also prone to the carrier recovery system's false locking onto the wrong quadrant of the modulated signal constellation, as detailed in [83]. Again, the non-coherently detected DAPSK solutions dispensed with a high pilot-overhead and eliminated the above-mentioned synchronization problems with the aid of so-called rotationally invarian constellations, while transmitting an increased number of bits/symbol [40, 41, 83]. These schemes, which have recently received an increasing attention from the communication community owing to their low decoding complexity and low peak power, will be discussed in Section IV-A, where we design a low-complexity near-optimum MSDD receiver for bandwidth-efficient single-transmit-antenna-assisted systems.

On the other hand, when considering the employment of non-constant-modulus constellation for DUSTM-based MIMO systems in pursuit of high spectrum efficiency, DUSTM using APSK and QAM constellations, which have an increased minimum Euclidean distance over the PSK constellation, were proposed in [86] and [87], respectively. However, in constrast to the single-transmit-antenna differential system, the DUSTM mechanism allows an easy employment of the sqaure QAM constellation, which will be considered instead of APSK in Section IV-B2 regarding the low-complexity near-optimum MSDD design for high-spectrum-efficiency MIMO systems. This is because that square QAM has a larger Euclidean distance between the constellation symbols than the APSK, thus implying a superior noise performance [88].

A. Design of MSDSD for SISO Systems Using DAPSK

In order to eliminate the typical emergence of an error-floor at high Doppler-frequencies, the application of the full-search-based ML-MSDD discussed in Section III-B1 has been extended to uncoded DAPSK-modulated system in [75] as well as to channel-coded DAPSK reception basded on the MAP criterion in [89]. However, since the constellation size of DAPSK is typically no smaller than 16 in bandwidth-efficient communications, the ML-MSDD employing even a moderate observation window size of $N_{\rm wind}$ may exhibit an excessive complexity. In order to reduce the potentially excessive complexity, the DF-DD scheme of [42] has been developed for the DAPSK system, which, however, may suffer from a moderate but non-negligible performance loss owing to its inherent vulnerability to feedback error propagation. As another promising complexity reduction technique, the SD mechansim has also been proposed for MSDD of conventional DPSK, as reviewed in Section III-B2, leading to the MSDSD scheme. Unfortunately, the non-constant-modulus constellation DAPSK precludes the direct application of the MSDSD scheme of [90]. Therefore, the conception of an efficient MSDD for DAPSK systems invoking the SD mechanism has been a challenging open problem. Hence the solution of this problem may constitute a promising candidate for low-complexity near-optimum MSDD implementations.

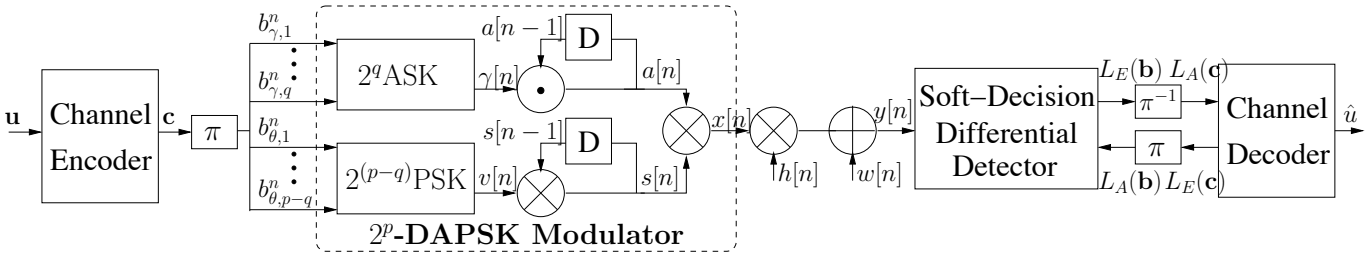

Figure 12. Overall system model of bit-interleaved coded 16-DAPSK over Rayleigh-fading channel.

Table IV
AMPLITUDE MAPPING FOR 16- AND 64-DAPSK

16-DAPSK ($q=1$)				**64-DAPSK** ($q=2$)					
$a[n]$		$b^n_{\gamma,1}$		$a[n]$		$b^n_{\gamma,1}, b^n_{\gamma,2}$			
		0	1			00	01	11	10
		$\gamma[n]$				$\gamma[n]$			
		1	α			1	α	α^2	α^3
$a[n-1]$	1	1	α	$a[n-1]$	1	1	α	α^2	α^3
					α	α	α^2	α^3	1
	α	α	1		α^2	α^2	α^3	1	α
					α^3	α^3	1	α	α^2

1) Differential Amplitude and Phase Shift Keying: Here we consider a bit-interleaved coded differential modulation SISO design example of Fig. 12 employing the iterative detection (ID) mechanism. At the transmitter a block of L information bits $\mathbf{u}$ is first encoded by the channel encoder in order to generate the coded bits $\mathbf{c}$, which are then interleaved by the interleaver π. The resultant permuted bits $\mathbf{b}$ are then fed through the DAPSK modulator. The 2^p-DAPSK employs multiple concentric rings by combining the 2^q-DASK and $2^{(p-q)}$-DPSK modulation schemes. As illustrated in Fig. 12, the first q bits, $\mathbf{b}^n_\gamma = [b^n_{\gamma,1}, \cdots, b^n_{\gamma,q}]$, of the nth p-bit encoded APSK symbol $d[n] = \gamma[n]v[n]$ are mapped to one of the legitimate radii $\mathcal{R} = \{\alpha^{i_\mathrm{A}} |\ i_\mathrm{A} = 0, \cdots, 2^q - 1\}$ in order to generate the component ASK symbol $\gamma[n]$. Meanwhile, the remaining $(p-q)$ bits, $\mathbf{b}^n_\theta = [b^n_{\theta,1}, \cdots, b^n_{\theta,p-q}]$, are mapped to the component PSK symbol $v[n] = \mathrm{e}^{j\theta[n]} \in \mathcal{V} = \{\mathrm{e}^{j2\pi i_\mathrm{P}/2^{(p-q)}} | i_\mathrm{P} = 0, \cdots, 2^{(p-q)} - 1\}$. Then, the differential amplitude and phase modulation processes are carried out in parallel, as observed in Fig. 12. More particularly, during the amplitude differential modulation the current amplitude state $a[n]$ is chosen from the constellation diagram depending on the previous amplitude state $a[n-1]$, taking into account the ASK symbol $\gamma[n]$ according to Table IV. Finally, the DAPSK symbol $x[n]$ may be generated as the product of the DASK and DPSK symbols according to $x[n] = a[n]s[n]$. As an example, the signal constellation set $\mathcal{M}_c$ of 16-DAPSK ($p = 1,\ q = 4$) is depicted in Fig. 13.

2) MAP-Based MSDD for DAPSK: In the light of the generalized multiple-symbol system model of (3), we may straightforwardly obtain the multiple-symbol system model for the DAPSK modulated system of Fig. 12 as $\underline{\mathbf{Y}}[k_N] = \underline{\mathbf{X}}^\mathrm{d}[k_N]\underline{\mathbf{H}}[k_N] + \underline{\mathbf{W}}[k_N] = \underline{\mathbf{A}}^\mathrm{d}[k_N]\underline{\mathbf{S}}^\mathrm{d}[k_N]\underline{\mathbf{H}}[k_N] + \underline{\mathbf{W}}[k_N]$, where $\underline{\mathbf{X}}^\mathrm{d}[k_N]$, $\underline{\mathbf{A}}^\mathrm{d}[k_N]$ and $\underline{\mathbf{S}}^\mathrm{d}[k_N]$ are all diagonal matrices containing the kth block of N_wind consecutively transmitted DAPSK symbols, ASK symbols as well as PSK symbols along their diagonal, respectively.

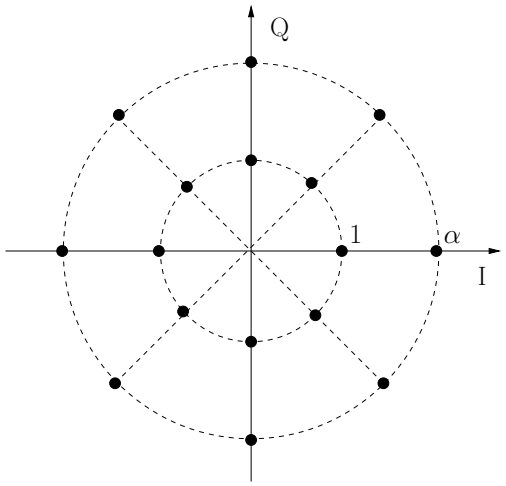

Figure 13. Signal constellation of 16-DAPSK (α denotes the ring ratio).

Based on the above multiple-symbol system model, the MSDD discussed in Sction III-B1 may be directly applied to the single-transmit-antenna-assisted DAPSK system. However, we have to bear in mind that since the conditional PDF $p(\underline{\mathbf{Y}}[k_N]|\underline{\mathbf{X}}^\mathrm{d}[k_N])$ is dependent on the amplitude of the non-constant-modulus reference symbol x_ref (i.e. on the first upper-left element of the diagonal matrix $\underline{\mathbf{X}}^\mathrm{d}[k_N]$), the metric employed in the MSDD, namely, the conditional PDF $p(\underline{\mathbf{Y}}[k_N]|\mathbf{b}[k_N]) = p(\underline{\mathbf{Y}}[k_N]|\mathbf{\Gamma}[k_N], \mathbf{\Theta}[k_N])$ should be caculated by averaging $p(\underline{\mathbf{Y}}[k_N]|\underline{\mathbf{X}}^\mathrm{d}[k_N])$ over all possible values of x_ref as $p(\underline{\mathbf{Y}}[k_N]|\mathbf{\Gamma}[k_N], \mathbf{\Theta}[k_N]) = E_{x_\mathrm{ref}}\{p(\underline{\mathbf{Y}}[k_N]|\underline{\mathbf{X}}^\mathrm{d}[k_N])\}$, where $\mathbf{\Gamma}[k_N] = [\gamma[k(N_\mathrm{wind} - 1)], \cdots, \gamma[(k+1)(N_\mathrm{wind} - 1) - 1]]^\mathrm{T}$ and $\mathbf{\Theta}[k_N] = [\theta[k(N_\mathrm{wind} - 1)], \cdots, \theta[(k+1)(N_\mathrm{wind} - 1) - 1]]^\mathrm{T}$ correspond to the k_Nth block of consecutively transmitted $(N_\mathrm{wind} - 1)$ pieces of the amplitude-ratio and phase-rotation information, respectively. The soft bit information expressed in terms of *a posteriori* LLRs may then be calculated with the aid of Bayes' theorem at the output of the MAP-MSDD as (again, the block index k_N is omitted for notation simplicity):

$$L_D(b^n_i|\underline{\mathbf{Y}}) = \ln \frac{\sum_{\mathbf{b}\in\mathbb{B}_{n,i,+1}} p(\underline{\mathbf{Y}}|\mathbf{\Gamma}, \mathbf{\Theta})\Pr(\mathbf{b})}{\sum_{\mathbf{b}\in\mathbb{B}_{n,i,-1}} p(\underline{\mathbf{Y}}|\mathbf{\Gamma}, \mathbf{\Theta})\Pr(\mathbf{b})}, \qquad (4)$$

where $\mathbb{B}_{n,i,\pm 1}$ represents the set of $2^{(pN-1)}$ legitimate transmitted bit vectors $\mathbf{b}$ associated with the ith bit of the nth p-bit-coded symbol being $b^n_i = \pm 1$ ($i \in \{0, \cdots, p-1\}$).

According to (4), the asymptotic complexity of the MAP-MSDD of a 2^p-DAPSK scheme using 2^q concentric rings is

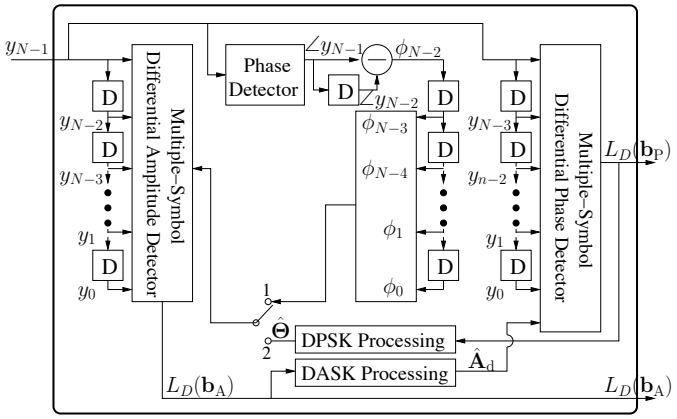

Figure 14. Iterative multiple-symbol differential amplitude/phase detection (Illustration for the first multiple-symbol block, i.e., $k_N = 0$).

$\mathcal{O}(p \cdot 2^{(pN)})$. Therefore, employing the ML - search carried out by the MAP-MSDD might impose a potentially excessive computational complexity and hence may preclude its practical implementation, especially for high-order modulation schemes and/or for high observation window sizes.

3) The Design of Iterative Amplitude/Phase MSDSD: Since the transmitted signal matrix $\underline{\mathbf{X}}^{\mathrm{d}}$ is no longer unitary in the DAPSK modulated system, we are unable to transform the maximization problem of the ML-MSDD decision metric into an efficient SD-aided layered tree search, as it was observed in Section III-B2 for the DPSK modulated scenario. As another approach of reducing the complexity, the idea of decoupling the joint amplitude and phase detection was conceived in [91] for MSDD invoked for DAPSK modulated transmission over Rayleigh channels. Regretfully, this sub-optimum scheme only achieved a complexity reduction at the cost of a significant performance loss.

In order to recover from this potentially substantial performance degradation, below a novel IAP-MSDSD mechanism is proposed for channel coded DAPSK modulated systems. As illustrated in Fig. 14, N_{wind} consecutively received symbols are collected and fed through the decoupled serially concatenated multiple-symbol differential amplitude detector (MSDAD) and multiple-symbol differential phase detector (MSDPD) of Fig. 14. We note that the soft-decision-based detection of the amplitude- and phase-modulation-related bits is conducted independently and their generated soft amplitude and phase information may be iteratively exchanged between each other. The decoupling of the amplitude and phase detection renders the SD mechanism applicable to the computationally demanding MSDPD process of acquiring the phase estimate $\hat{\underline{\mathbf{S}}}^{\mathrm{d}}$, which uses the amplitude estimates of the consecutively transmitted symbols provided by the MSDAD as *a priori* information. The step-by-step operation of IAP-MSDSD is briefly summarized as follows:

Step 1: The IAP-MSDD process commences by obtaining the phase information $\hat{\mathbf{\Theta}}$ based on the output of the phase detector as $\hat{\mathbf{\Theta}} = [\phi_0, \cdots, \phi_{(N-1)}]^T$ by toggling the phase information feedback switch to the '1' location of Fig. 14, in order to provide the initial phase estimates $\hat{\mathbf{\Theta}}$ for the first round of MSDAD detection.

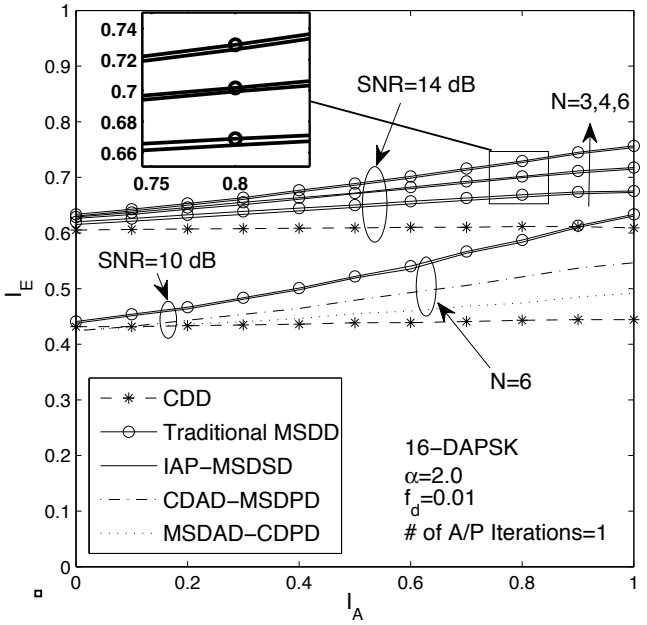

Figure 15. EXIT chart of the IAP-MSDSD employed in the 16-DAPSK system.

Step 2: In the presence of the estimated transmit-domain phase information $\hat{\mathbf{\Theta}}$, the *a posteriori* amplitude-modulation-related bit LLRs are computed by the MSDAD as:

$$L_D(b^n_{\gamma,i}|\underline{\mathbf{Y}}, \hat{\mathbf{\Theta}}) = \ln \frac{\sum_{\mathbf{b}_\gamma \in \mathbb{B}^\gamma_{n,i,+1}} p(\underline{\mathbf{Y}}|\mathbf{\Gamma}, \hat{\mathbf{\Theta}}) \Pr(\mathbf{b}_\gamma)}{\sum_{\mathbf{b}_\gamma \in \mathbb{B}^\gamma_{n,i,-1}} p(\underline{\mathbf{Y}}|\mathbf{\Gamma}, \hat{\mathbf{\Theta}}) \Pr(\mathbf{b}_\gamma)}, \quad (5)$$

where $\mathbb{B}^\gamma_{n,i,\pm 1}$ represents the set of $2^{[q(N-1)-1]}$ legitimate amplitude-modulation-related bit vectors $\mathbf{b}_\gamma$ associated with $b^n_{\gamma,i} = \pm 1$ ($i \in \{1, \cdots, q\}$).

Step 3: Subsequently, the amplitudes $\hat{\underline{\mathbf{A}}}^{\mathrm{d}}$ of the consecutively transmitted symbols may be estimated based on the *a posteriori* amplitude-modulation-related bit LLRs, i.e. $L_D(\mathbf{b}_\gamma|\mathbf{y}, \hat{\mathbf{\Theta}})$ of (5), which are then delivered to the serially concantenated MSDPD.

Step 4: Thanks to the amplitude estimate matrix $\hat{\underline{\mathbf{A}}}^{\mathrm{d}}$, the *a posteriori* phase-modulation-related bit LLRs may be computed by the MSDPD of Fig. 14, where the efficient SD mechanism can be incorporated in a similar manner as seen in Section III-B2.

Step 5: From the second iteration of the MSDAD process onwards, the phase information feedback switch of Figure 14 is toggled to the '2' position in order to exploit the phase-modulation-related bit LLRs delivered by the MSDPD. Then, go back to Step 2, if further iterative A/P detection is required.

Step 6: Output both the amplitude- and phase-modulation-related bit LLRs $L_D(\mathbf{b}_{\mathrm{A}})$ and $L_D(\mathbf{b}_{\mathrm{P}})$.

4) Application Example - 16DAPSK SISO System: Let us now invoke the semi-analytical EXtrinsic Information Transfer (EXIT) charts of [92] for investigating the performance versus complexity of the IAP-MSDSD scheme conceived for the single-antenna-aided 16-DAPSK-modulated SISO system of

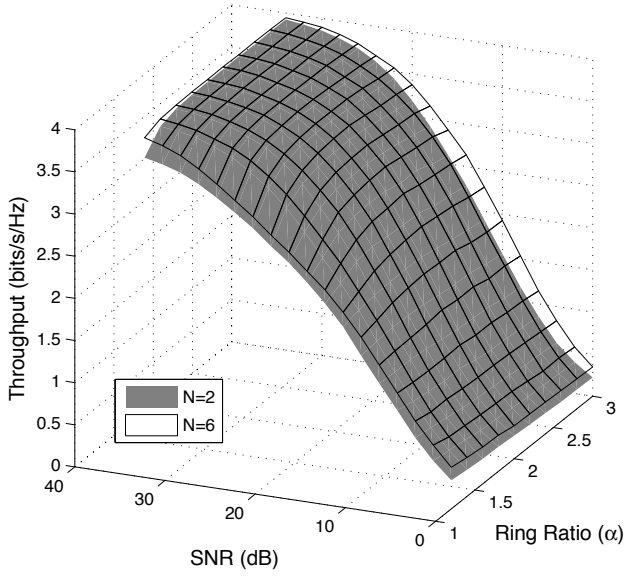

Figure 16. Maximum achievable throughput of the 16-DAPSK system.

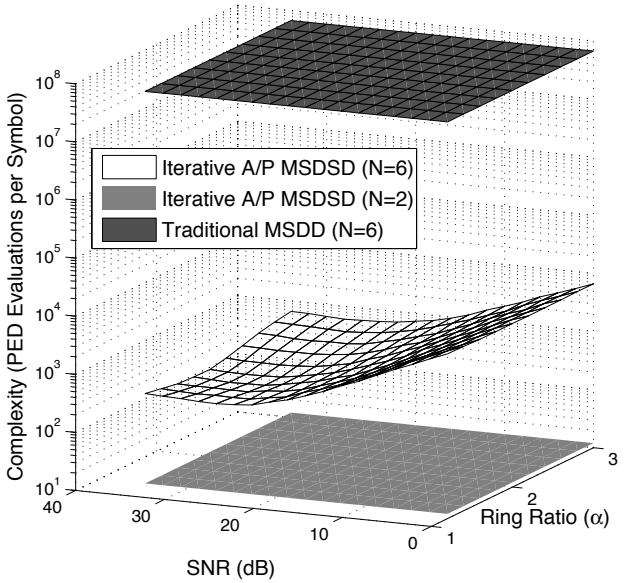

Figure 17. Complexity reduction achieved by the IAP-MSDSD in the 16-DAPSK system.

Fig. 12 experiencing a normalized Doppler frequency of $f_d = 0.01$. According to the area properties of the EXIT chart [92], the upwards-shifted EXIT curve of the IAP-MSDSD in Fig. 15 suggests that a significantly higher maximum transmission rate may be achieved in comparison to the CDD assisted system using $N_{\rm wind} = 2$. This throughput gain was achieved by jointly detecting $N_{\rm wind} > 2$ data symbols using the IAP-MSDSD, as also visualized in the 3D plot of Fig. 16, where the maximum achievable throughput of the IAP-MSDSD-aided 16-DAPSK modulated system is portrayed versus both the SNR and the ring-ratio α. Additionally, a compromise between the achievable performance and the complexity imposed may be struck by employing the low-complexity conventional differential amplitude detection (CDAD) or conventional differential phase detection (CDPD) philosophy in the corresponding amplitude or the phase detection process, as indicated by the associated downwards-shifted dotted and dot-dashed EXIT curves of Fig. 15. Moreover, as implied by the almost invisible gap between the EXIT curve of the IAP-MSDSD and that of the traditional MSDD seen in Fig. 15, both the MSDAD and MSDPD of the IAP-MSDSD of Fig. 14 has to be activated only once, in order to approach the performance of the traditional MSDD. Thus, remarkably, the complexity imposed by the IAP-MSDSD becomes about five orders of magnitude lower than that of the traditional MSDSD for the 16-DAPSK modulation-aided system across a wide range of SNRs, as seen in Fig. 17, where the complexity quantified in terms of the number of transmitted symbol vector candidate enumerations during the differential detection is portrayed versus both the SNR and the ring-ratio α. Furthermore, the simulation results seen in Figs. 16 and 17 suggest that setting the ring-ratio employed by the 16-DAPSK to $\alpha \approx 2.0$ constitutes an appropriate choice for maximizing the achievable throughput [93], while minimizing the complexity imposed.

B. Design of MSDSD for MIMO Systems Using QAM-DUSTM

1) DUSTM Using QAM Constellations: In contrast to the traditional space-time block coding (STBC) framework, the DUSTM structure portrayed in Fig. 4 introduces a differential encoding unit, in order to forgo the burden of channel estimation. However, the differential encoding structure imposes a unitary constraint on the resultant space-time coded matrices, otherwise the matrix product $\mathbf{S}[n] = \mathbf{V}[n]\mathbf{V}[n-1]\cdots\mathbf{V}[1]$ may become zero, infinity or possibly both in different spatial and temporal directions, as the differential space-time encoding proceeds. In other words, the challenge of designing DUSTM can be described as that of designing a family of STBCs, where all the space-time matrices are unitary. A straighforward way of designing DUSTM is based on Alamouti codes [6], where the challenge of constructing a set of unitary space-time matrices $\mathbf{V}[n]$ for the schematic of Fig. 4 is tackled by simply employing, for example, the well-known $\mathbf{G}_2$ matrices with their elements drawn from a 2^p-PSK constant-modulus constellation.

Let us now briefly review how the PSK constellation can be replaced by its non-constant-modulus square QAM counterpart, while still preventing the peak power of the transmitted signals generated by the DUSTM encoding process from becoming infinity or zero. The reader's familiarity with the Alamouti STBC is assumed here. Then we consider a co-located MIMO system equipped with two transmit antennas as our design example. Thus the $\mathbf{G}_2$-based DUSTM encoding process may be formulated as $\mathbf{S}[n] = \frac{1}{\eta_{n-1}}\mathbf{S}[n-1]\mathbf{V}[n] = \frac{1}{\eta_{n-1}}\mathbf{S}[n-1]\mathbf{G}_2(v_1[n], v_2[n])$, where the function $\mathbf{G}_2(\cdot)$ takes two input symbols drawn from the 2^p-QAM constellation for generating the associated (2×2)-dimensional space-time matrix. The first transmitted space-time signal is also a $\mathbf{G}_2$ matrix, which serves as the reference symbol. Furthermore, it

is the power normalization factor $\eta_{n-1} = \sqrt{||\mathbf{S}[n-1]||^2/2} = \sqrt{|v_1[n-1]|^2 + |v_2[n-1]|^2}$ that is introduced for confining the peak power of the transmitted signals after differential encoding within a certain limit.

In order to recover the QAM symbols $(v_1[n], x_2[n])$ using the CDD, which performs ML detection based on low-complexity linear processing, both the transmit power normalization factor η_n and the fading channel's power envelope has to be known by the receiver. The factor η_n may be directly obtained from the previous decisions, but the fading channel's power envelope has to be estimated, for example, by evaluating the auto-correlation of the received signal. Naturally, the accuracy of this estimation highly depends on both the estimation window duration as well as on the Doppler frequency. Since the implementation of the related ML detection is a well-known standard process, we refer the interested reader to [87] for more details and continue our discourse focusing on how to efficiently carried out multiple-symbol-based detection for the DUSTM system using QAM constellations for the sake of enhancing its robustness against rapid channel fluctuation.

2) The Design of MSDSD for QAM-Based DUSTM: By constructing the multiple-symbol system model of (3) detailed in Section III-A1 for the QAM-based-DUSTM system, the ML-MSDD discussed in Section III-B1 can be directly applied. However, a problem precludes the direct application of the SD regime for reducing the ML-MSDD's excessive complexity experienced in the context of QAM-based DSTUM MIMO systems, which was also encountered in the DAPSK-aided SISO scenario. This specific problem is that the matrix $\underline{\mathbf{S}}^{\mathrm{d}}$ of (3) encapsulating the consecutively transmitted space-time signals is no longer unitary. Furthermore, another challenging problem faced by the SD algorithm when aiming for complexity reduction is the estimation of the power normalization factor η_n. Therefore, we will highlight three major actions enabling an efficient implementation of the ML-MSDD relying on the SD mechanism in our following discourse:

Action 1 - *Generation of Equivalent Unitary Signal Matrix and Its Associated Channel Matrix:* In the light of our multiple-symbol system model of (3) let us consider the first transmission block as an example, where we may have $\tilde{\underline{\mathbf{S}}}^{\mathrm{d}} = \mathrm{diag}\{\frac{1}{\sqrt{2}\eta_1}\mathbf{S}[1] \cdots \frac{1}{\sqrt{2}\eta_{N_{\mathrm{wind}}}}\mathbf{S}[N_{\mathrm{wind}}]\}$ and $\tilde{\underline{\mathbf{H}}} = [\sqrt{2}\eta_1\mathbf{H}[1]^{\mathrm{T}} \cdots \sqrt{2}\eta_{N_{\mathrm{wind}}}\mathbf{H}[N_{\mathrm{wind}}]^{\mathrm{T}}]^{\mathrm{T}}$. The so-called *equivalent unitary signal matrix* $\tilde{\underline{\mathbf{S}}}^{\mathrm{d}}$ is specifically constructed in order to satisfy the above-mentioned unitary-matrix based prerequisite of incorporating the SD mechanism.

Action 2 - *Estimation of the Power Normalization Factor:* Since the first transmitted symbol of each detection block constitutes *a priori* knowledge, as we mentioned above, we re-order the layered signal detection process by rearranging each matrix of (3) upside down. Then, we now have $\tilde{\underline{\mathbf{H}}} = [\sqrt{2}\eta_{N_{\mathrm{wind}}}\mathbf{H}[N_{\mathrm{wind}}]^{\mathrm{T}} \cdots \sqrt{2}\eta_1\mathbf{H}[1]^{\mathrm{T}}]^{\mathrm{T}}$ for example. In the sequel, thanks to the layered tree search mechanism of the SD scheme, we can now embark on a joint detection of the transmitted symbol $\mathbf{S}_n$ and its associated normalization factor $\eta_n = \sqrt{||\mathbf{S}_n||^2/2}$, since the previous transmission matrix estimates $\{\hat{\mathbf{S}}_j\}_{j=1}^{n-1}$ as well as their associated transmit power normalization factor estimates $\{\hat{\eta}_j\}_{j=1}^{n-1}$ have already been temporarily obtained from the previous tree search phases.

Action 3: - *Construction of Partial Upper-Triangular Matrix:* Unfortuntely, the upper-triangular matrix $\tilde{\underline{\mathbf{U}}}$ used in the layered tree search of the SD scheme, which is obtained based on the channel's covariance matrix $\tilde{\Sigma}_h = E\{\tilde{\underline{\mathbf{H}}}\tilde{\underline{\mathbf{H}}}^{\mathrm{H}}\}$ may not be acquired, until all the decisions concerning the power normalization factors $\{\hat{\eta}_j\}_{j=1}^{N_{\mathrm{wind}}}$ have been attained. However, we found that a so-called partial upper-triangular matrix $\tilde{\tilde{\underline{\mathbf{U}}}}$ of $(nN_{\mathrm{t}}N_{\mathrm{r}}) \times (nN_{\mathrm{t}})$ elements may be generated based on the $(nN_{\mathrm{t}}) \times (nN_{\mathrm{t}})$-element partial channel covariance matrix $\tilde{\tilde{\Sigma}}_h$, which corresponds to the partial equivalent channel matrix $\tilde{\tilde{\underline{\mathbf{H}}}}$ obtained by removing the first $(N_{\mathrm{wind}} - n)$ rows of the complete channel matrix $\tilde{\underline{\mathbf{H}}}$. Furthermore, we observed that the partial upper-triangular matrix $\tilde{\tilde{\underline{\mathbf{U}}}}$ constitutes a matrix which is identical to the lower-right submatrix of the complete upper-triangular matrix $\tilde{\underline{\mathbf{U}}}$ used by the conventional SD algorithm, as illustrated in Fig. 18. This is equivalent to saying that the candidate search for the $(n+1)$st transmitted symbol may be carried out based on the partial upper-triangular matrix $\tilde{\tilde{\underline{\mathbf{U}}}}$, which is associated with the estimates of $\{\hat{\eta}_j\}_{j=1}^{n}$ that become available after the layered tree search for the previous n consecutively transmitted symbols. More explicitly, this is achieved without acquiring all the decisions of the power normalization factors $\{\hat{\eta}_j\}_{j=1}^{N_{\mathrm{wind}}}$. Consequently, as the tree search of the SD continues, the dimension of the partial upper-triangular matrix $\tilde{\tilde{\underline{\mathbf{U}}}}$ increases, and finally becomes the complete matrix $\tilde{\underline{\mathbf{U}}}$, when the layered tree search is completed.

3) Application Example - G2-DUSTM-16QAM System: In this section, we examine the performance of the proposed MSDSD scheme in the context of the two-transmit-antenna-aided $\mathbf{G}_2$-DUSTM-16QAM system. Its BER performance is portrayed in Fig. 19(a). It can be seen that the error floor of the CDD imposed by rapidly fading channels is successfully mitigated by the proposed MSDSD. We note that the MSDSD associated with $N_{\mathrm{wind}} = 2$ is equivalent to the CDD. Furthermore, as the MSDSD window duration N_{wind} increases, the performance of the noncoherent receiver approaches that of the idealized coherent scheme relying on perfect CSI estimation apart from the irreducible 3 dB gap, as evidenced by Fig. 19(a).

Fig. 19(b) presents our complexity comparison between the MSDD and the MSDSD, which is simply quantified as the number of 16-QAM constellation points visited by the MSDD/MSDSD per detected DUSTM information matrix. As seen in Fig. 19(b), the ML MSDD imposes a constant but potentially excessive complexity, even if the observation window size of $N_{\mathrm{wind}} = 3$ is only slightly higher than the $N_{\mathrm{wind}} = 2$ value employed by the CDD. On the other hand, the complexity imposed by the proposed MSDSD is a function of both the observation window size N_{wind} and the received SNR. As the SNR increases, the MSDSD's complexity decreases steadily and finally becomes comparable to that of the MSDSD in conjunction with $N_{\mathrm{wind}} = 2$.

V. Differential Interference Suppression Based on Joint Multiple-Symbol Filtering and Detection

Apart from the high-order modulation schemes discussed in the previous sections, a more promising solution to achieve

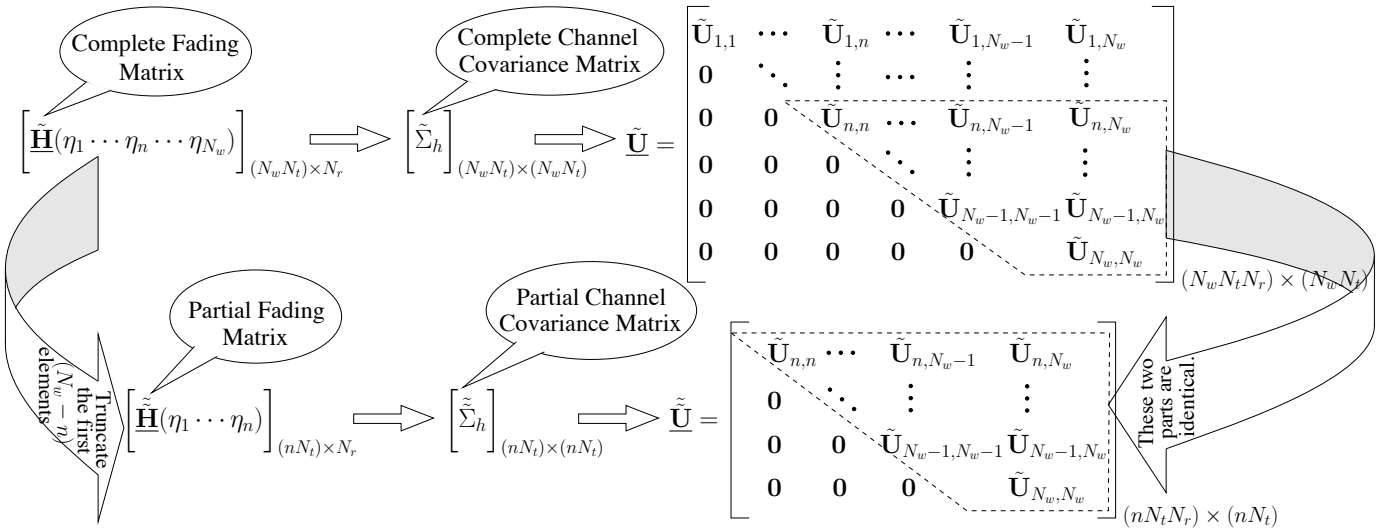

Figure 18. Generation of the partial upper-triangular matrix $\tilde{\underline{\mathbf{U}}}$ and its properties.

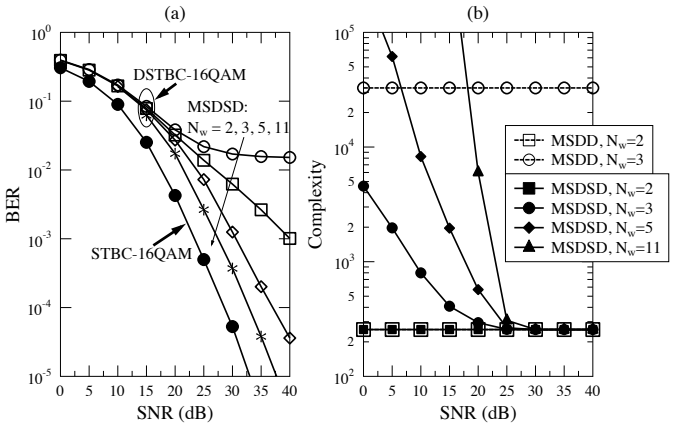

Figure 19. BER performance and Complexity of MSDSD aided DUSTM employing 16QAM, for $f_d = 0.03$.

a significantly improved bandwidth-efficiency is the non-orthogonal transmission based on the exploitation of the spatial dimension. Explicitly, we may employ spatial division multiple access (SDMA) [1], where the user-specific CIRs are estimated and invoked for differentiating the parallel UL streams transmitted by the different users. Regretfully, it was revealed in [94] that the SDMA system's performance is highly sensitive to the channel estimation errors, which may only be mitigated at the cost of an excessive computational complexity and/or high pilot overheads in many practical time-varying fading scenarios. Fortunately, however, it is possible to circumvent the channel estimation. This may be achieved by estimating and cancelling the multiple-access interference with the aid of an appropriately designed adaptive receiver. For example, the adaptive minimum mean square error (MMSE) scheme [95] using the least mean square (LMS) or the recusive least squares (RLS) algorithm and the more recently proposed maximum signal-to-interference-plus-noise ratio (MSINR) based differential interference suppression (DIS) scheme [96] may be invoked. For the LMS scheme the interference suppression filter has to be adapted in an agile manner, in order to minimize the MSE between the transmitted signal and the filter's output signal, while for the MSINR solution the filter coefficients are adjusted to maximize the SINR at its output. It has been demonstrated in [96] the MSINR solution is also capable of mitigating the effects of carrier phase variations.

A. Multiple-Symbol SDMA-OFDM System Model

In the context of nonorthogonal transmissions, the signals transmitted from multiple MSs are superimposed on each other at the receive antennas, thus the per-sub-carrier-based multiple-symbol SDMA-OFDM system is formulated on the basis of its orthogonal-transmission counterpart of (3) as:

$$\underline{\mathbf{Y}}[k_N] = \sum_{u=1}^{U} \underbrace{\underline{\mathbf{S}}_u^{\mathrm{d}}[k_N]\underline{\mathbf{H}}_u[k_N]}_{\underline{\mathbf{Y}}_u[k_N]} + \underline{\mathbf{W}}[k_N], \tag{6}$$

where the subscript u is introduced here to differentiate the terms associated with each MS while the sub-carrier index is again omitted here for notational simplicity. The dimension of each term in (6) is in line with that of the corresponding term of (3). Due to pratical cost- and size- constraints, the employment of a single transmit antenna is assumed for each MS without loss of generality, i.e. we have $N_{\mathrm{t}} = 1$. In order to circumvent the channel estimation, the uth single-antenna-aided MS differentially encodes its information symbols $\mathbf{V}_u[n] \in \mathcal{M}_c = \{e^{j2\pi m/M}; m = 0, 1, \cdots, M-1\}$, each of which contains $(\log_2 M)$-bit information, as $\mathbf{S}_u[n] = \mathbf{V}_u[n]\mathbf{S}_u[n-1]$, resulting in the so-called differential SDMA (DSDMA) system.

B. Adaptive Multiple-Symbol Differential Interference Suppression

It is observed from (6) that non-coherent differential detection techniques cannot be directly applied at the BS to recover the information pertaining to a specific MS without suppressing the interference imposed by all the other MSs. Therefore, we will use the MSINR approach of [96] for interference suppression in the DSDMA-OFDM system. However,

rather than computing the uth MS's linear vector filter $\mathbf{f}_u[n]$ of a specific sub-carrier for each OFDM symbol duration n, we propose updating $\mathbf{f}_u[k_N]$ only once for N_{wind} OFDM symbol durations based on the most recently received N_{wind} signal matrices hosted by $\underline{\mathbf{Y}}[k_N]$ of (6). The resultant new multiple-symbol MSINR (MS-MSINR) criterion reduces the filter-update overhead and additionally facilitates the implementation of the powerful MSDSD in the ensuing stage, hence achieving significant performance improvements.

1) Multiple-Symbol MSINR Criterion: Our goal is to find the specific filter $\mathbf{f}_v[k_N]$ capable of maximizing the filter's output SINR, which may be mathematically expressed as:

$$\mathbf{f}_v[k_N] = \max_{\mathbf{f}_v[k_N]} \frac{\mathbf{f}_v^{\text{H}}[k_N]\mathbf{R}[k_N]\mathbf{f}_v[k_N]}{\mathbf{f}_v^{\text{H}}[k_N]\mathbf{R}_v^i[k_N]\mathbf{f}_v[k_N]}, \tag{7}$$

where $\mathbf{R}[k_N] \triangleq E\{\underline{\mathbf{Y}}^{\text{H}}[k_N]\underline{\mathbf{Y}}[k_N]\}$ is the correlation matrix of the multiple-symbol-based received signal $\underline{\mathbf{Y}}[k_N]$ of (6) and $\mathbf{R}_v^i[k_N] \triangleq E\{(\underline{\mathbf{Y}}[k_N] - \underline{\mathbf{Y}}_v[k_N])^{\text{H}}(\underline{\mathbf{Y}}[k_N] - \underline{\mathbf{Y}}_v[k_N])\}$ is the multiple-symbol-based interference-plus-noise correlation matrix. Using the method of Lagrange multipliers, we may solve (7) by maximizing $\mathbf{f}_v^{\text{H}}[k_N]\mathbf{R}[k_N]\mathbf{f}_v[k_N]$ under the constraint that the interference-plus-noise component $\mathbf{f}_v^{\text{H}}[k_N]\mathbf{R}_v^i[k_N]\mathbf{f}_v[k_N]$ is fixed, leading to a so-called generalized eigenvalue problem [97]:

$$\mathbf{R}[k_N]\mathbf{f}_v[k_N] = \lambda\mathbf{R}_v^i[k_N]\mathbf{f}_v[k_N], \tag{8}$$

where λ represents the real-valued Lagrange multiplier.

2) MS-MSINR-Based Differential Interference Suppression: Thanks to the differential encoding mechanism, despite dispensing with channel estimation in the DSDMA-OFDM system, the interference-plus-noise correlation matrix $\mathbf{R}_v^i[k_N]$ may be calculated by exploiting the differentially encoded transmission principles. To be specific, under the assumption of a relatively slow fading channel, the multiple-symbol-based interference-plus-noise correlation matrix $\mathbf{R}_v^i[k_N]$ may be approximately evaluated as $\mathbf{R}_v^i[k_N] \approx \mathcal{E}\{\underline{\mathbf{E}}_v^{\text{H}}[k_N]\underline{\mathbf{E}}_v[k_N]\}$, where the multiple-symbol-based interference-plus-noise signal matrix $\underline{\mathbf{E}}_v[k_N]$ is defined as $\underline{\mathbf{E}}_v[k_N] \triangleq \sqrt{\frac{1}{2}}(\underline{\mathbf{Y}}[k_N] - \underline{\tilde{\mathbf{V}}}_v^{\text{d}}[k_N]\underline{\mathbf{Y}}[k_N^{-1}])$ with the block index k_N^{-n} representing the kth block shifted backwards by n OFDM symbol durations and the $(N_t N_{\text{wind}} \times N_t N_{\text{wind}})$-element diagonal block matrix $\underline{\tilde{\mathbf{V}}}_v^{\text{d}}[k_N] = \text{diag}\{\underline{\tilde{\mathbf{V}}}_v[k_N]\} = \text{diag}\{[\mathbf{V}_v[(N_{\text{wind}} - 1)(k-1)]^T, \underline{\mathbf{V}}_v[k_N]^T]^T\}$ is the multiple-symbol-based transmitted information symbol matrix of the vth MS. The diagonal block matrix $\underline{\tilde{\mathbf{V}}}_v^{\text{d}}[k_N]$ is known to the receiver during the training session or may be estimated by using the previous decisions [98].

3) Adaptive Implementation of MS-DIS: In practice, rather than carrying out the high-complexity singular-value decomposition to solve the generalized eigenvalue problem of (8), we apply a multiple-symbol-version of the adaptive Newton algorithm of [99] for recursively updating the differential interference suppression (DIS) filter $\mathbf{f}_v[k_N]$. This modified adaptive Newton algorithm, which was shown in [99] to have a fast convergence and an excellent tracking capability[10] is omitted here owing to the lack of space - the interested reader is referred to [98, 99]. It is worth noting that in constrast to the conventional single-symbol based adaptive algorithm, the filter $\mathbf{f}_v[k_N]$ is updated at the beginning of each N_{wind}-OFDM-symbol block and it is used unaltered throughout the N_{wind}-OFDM-symbol block to suppress the multiple-access interference imposed by the other MSs. This block-based filtering regime facilitates the implementation of the MSDSD scheme as a benefit of imposing no further distortion on the phase difference between the consecutively transmitted symbols in addition to that caused by the time-varying fading channel.

C. MS-DSDMA Transceiver Design

We now consider a channel-code aided turbo DIS receiver for the DSDMA-OFDM system supporting U MSs, which is depicted in Fig. 20. Specifically, the BS receiver of Fig. 20 is constituted by three modules, namely the DIS filter bank, the MSDSD and the channel decoder, where the extrinsic information may be exchanged amongst the three concantenated components in a number of consecutive iterations. As shown in Fig. 20, $A(\cdot)$ represents the *a priori* information expressed in terms of the LLRs, while $E(\cdot)$ denotes the corresponding *extrinsic* information, whereas the labels u and c represent the uncoded and coded bits, respectively, corresponding to the specific module indicated by the subscript. Bearing in mind the goal of striking an attractive compromise between the attainable system performance and the complexity, our design guidelines may be summarized as follows:

a) Channel-Code-Aided Turbo DIS: At the early stage of the iterative detection process, $\underline{\tilde{\mathbf{V}}}_v[k_N]$ which is used for evaluating $\mathbf{R}_v^i[k_N]$ should be obtained based on the output of the MSDSD by toggling the decision-directed mode switch to the 'a' location of Fig. 20, in order to ensure that the system is operating in its decision-directed mode. However, as soon as the *a priori* information delivered by the channel decoder becomes more reliable during the iterative detection process, namely when we have $I_E(c_1) > I_E(u_2)$, it is preferred to switch to the "channel-code-aided" decision-directed mode by toggling the switch to the 'b' location in Fig. 20, so that $\underline{\tilde{\mathbf{V}}}_v[k_N]$ is calculated from the *a priori* information provided by the channel decoder.

b) Soft-Symbol-Decision-Direct DIS: Based on the idea of retaining the valuable soft-information contained in the *a posteriori* LLRs, which would be simply discarded by the action of subjecting the LLRs to hard decisions, soft-symbol-decision-directed (SSDD) DIS is advocated. In this context the soft- rather than hard-decision symbol is calculated based on the *a priori* LLRs delivered either by the MSDSD or by the channel decoder for $\underline{\tilde{\mathbf{V}}}_v[k_N]$.

c) Adaptive-Window-Duration Based MSDSD: Instead of using a fixed observation window size of N_{wind} during the entire iterative detection process, the observation window size

[10]Our investigations, which are omitted here owing to the lack of space, indicate that the MSINR-based DIS scheme exhibits a lower sensitivity to the quality of the feedback decision than that of its conventional RLS-LMMSE-based counterpart, resulting in a superior tracking capability.

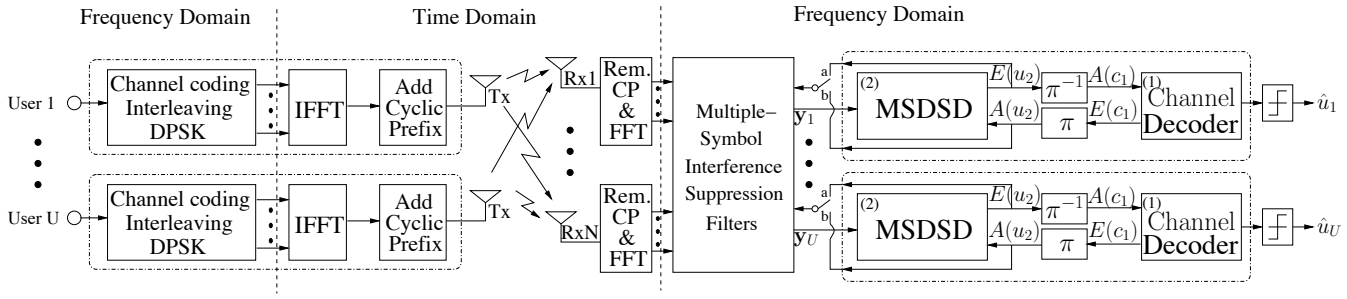

Figure 20. Multiple-symbol DSDMA-OFDM transceiver architecture.

Table V
SUMMARY OF SYSTEM PARAMETERS

Modulation	DQPSK in Time Domain
Users Supported	2
Normalized Doppler Freq.	0.001
System	DSDMA-OFDM Uplink
Sub-Carriers	1024
Rx at BS	2
Channel Code	Half-Rate RSC(2,1,3) (5/7)
TDL Channel Model	Typical Urban 6-Tap Channel Model
Channel Delay Profile	[0 2 6 16 24 50]

employed by the MSDSD was initially set to $N_{\text{wind}} = 2$ for the sake of a low complexity. However, this window-size will be slightly increased, as soon as the iterative decoding process exchanging extrinsic information between the combined "DIS-MSDSD" decoder and the channel decoder converges. The proposed AWD-aided MSDSD scheme is characterized with the aid of the EXIT chart seen in Fig. 21(a) in the context of a (2×2)-element DQPSK modulated DSDMA-OFDM system, where we may also observe the transition of the decision-directed mode from the MSDSD-based mode to the channel-code-based mode at the second iteration, as we discussed above. Indeed, the complexity imposed by the MSDSD is significantly reduced by the AWD scheme, as observed in Fig. 21(b), where the complexity imposed by the MSDSD in terms of the number of the PED evaluations per bit is plotted versus the SNR for the systems operating both with and without the AWD scheme.

d) Apriori-LLR-Threshold Aided MSDSD: Bearing in mind that the sign of the resultant LLRs indicates whether the current bit is more likely to be $+1$ or -1, whereas the magnitude reflects how reliable the decision concerning the current bit is, the search space of the MSDSD may be significantly reduced by invoking an ALT controlled technique. To be specific, when calculating the *a posteriori* LLR $L_D(b_i)$ for the ith bit component b_i of the bit vector $\mathbf{b}$, the vector candidates $\mathbf{b}$ associated with b_j $(j \neq i, j \in \mathcal{J})$ having values opposite to those indicated by the sign of their *a priori* LLRs may be excluded from the search space, as long as their *a priori* LLRs exhibit magnitudes higher than the preset threshold T_{ALT}. As seen in Fig. 21(b), the integration of ALT schemes ($T_{\text{ALT}} = 10$) further reduce the complexity of the MSDSD significantly without sacrificing the performance.

D. Simulation Results and Discussions

In Fig. 22 the BER performance of the proposed turbo MS-DIS-aided DSDMA system of Fig. 20 is plotted in comparison to those of its LMMSE-based and MSINR-based single-symbol-DIS-aided counterparts, in the specific context where two single-antenna-aided users are assumed to transmit simutaneously to the two-antenna-aided BS. The simulation parameters are summarized in Table V. It is observed in Fig. 22 that for $N_{\text{wind}} = 1$ the coded RLS-based-LMMSE DSDMA-OFDM system is slightly inferior to its MSINR-based counterpart in terms of its BER performance within the SNR range of interest. Furthermore, when the MS-DIS scheme operates in conjunction with $N_{\text{wind}} = 7$, the MSINR-based system using the ALT- and AWD-aided MSDSD is capable of achieving an SNR gain of 5 dB over its LMMSE-based counterpart at the BER target of 10^{-4} in the channel-coded scenario associated with $f_d = 0.001$. Finally, observe in Fig. 22 that the error-floor induced by a more severely time-selective channel may be significantly mitigated by the proposed MSINR-based MS-DIS scheme in conjunction with the ALT- and AWD-aided MSDSD. More specifically, an SNR gain of about 7 dB can be achieved by the proposed turbo MS-DIS-aided three-stage receiver employing $N_{\text{wind}} = 7$ in comparison to the conventional MSINR-based DIS-assisted system using $N_{\text{wind}} = 1$ in the time-varying fading channel associated with $f_d = 0.005$.

VI. CONCLUSIONS AND FUTURE RESEARCH

A. Summary and Conclusions

Multiple-symbol joint signal processing techniques, which are capable of exploiting the fading channel's memory, were advocated in this treatise as an appealing, practically implementable candidate for differentially modulated systems dispensing with the potentially excessive-complexity and yet inaccurate channel estimation. The benefits of the multiple-symbol joint signal processing include the enhancement of the system's robustness against rapid channel fluctuation, striking a flexible performance-complexity compromise by appropriately adapting the observation window size N_{wind} as well as the provision of enhanced iterative gains achieved for channel-code-aided iterative receivers. As a prominent scheme in the family of multiple-symbol signal processing techniques conceived for differential signalling systems, the ML MSDD and its SD-based reduced-complexity counterpart, namely MSDSD, were briefly reviewed based on our generalized MIMO-OFDM multiple-symbol transmission model of

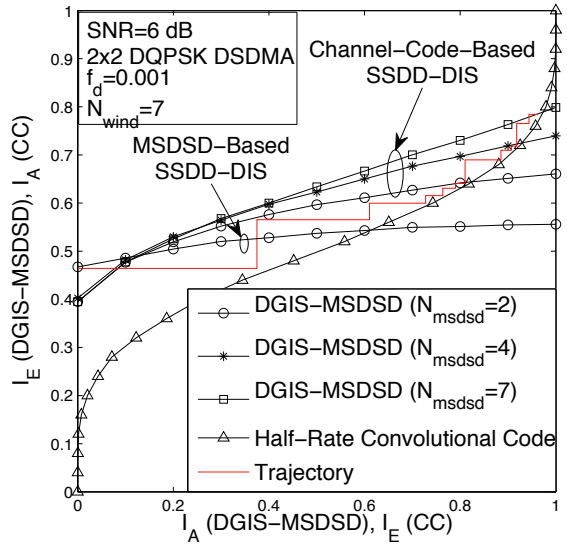

(a) EXIT trajectory.

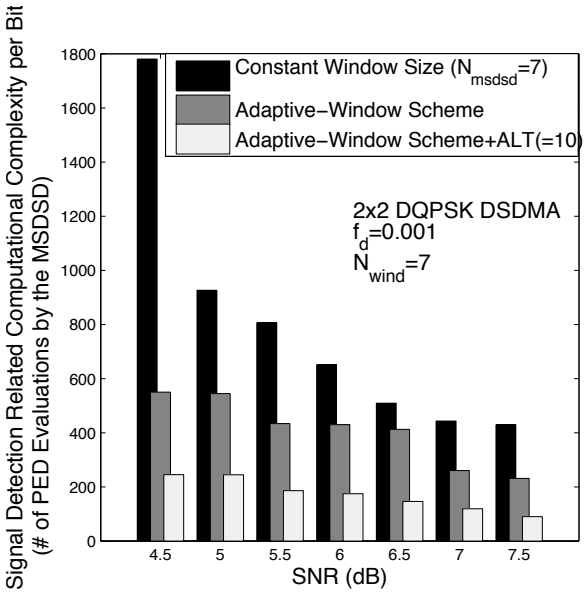

(b) Complexity reduction achieved.

Figure 21. Characterization of the adaptive-window aided scheme for the MSDSD.

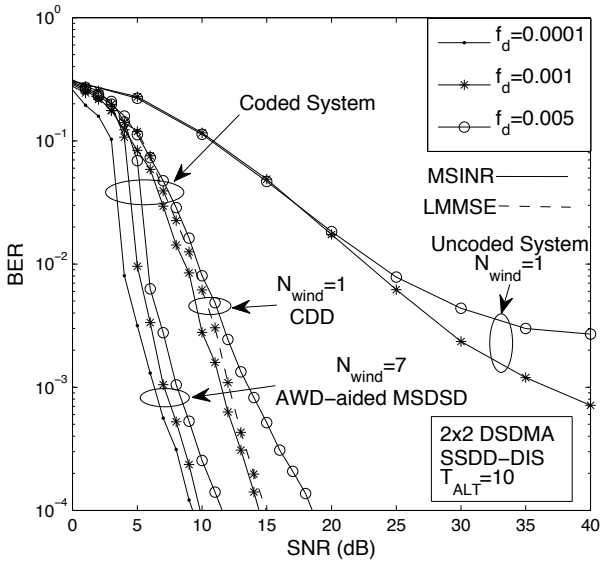

Figure 22. BER performance of the MS-DSMA OFDM system using the ALT- and AWD-aided MSDSD.

Section III, which subsumes the SISO system as a special case. However, our discussions of multiple-symbol signal processing was not restricted to the family of differentially modulated systems relying on conventional constant-modulus constellations. Instead, communication systems using nonconstant-modulus constellation based signaling mechanisms, such as the DAPSK and the DUSTM-QAM schemes were considered, in the interest of more efficiently exploiting the scarce spectral resources for accommodating the ever-increasing traffic demands. Although the exhaustive-search-based MSDD mechanism is directly applicable to the above high-order differential modulation schemes, they exhibit a potentially excessive complexity, which is increased exponentially both with the modulation constellation size and with the multiple-symbol processing block size. The bottleneck of efficiently implementing the MSDD for the DAPSK and DUSTM-QAM schemes lies in the fact that the employment of the nonconstant-modulus constellation destroys the unitary nature of the transmitted multiple-symbol signal matrix. Therefore we transplanted the SD regime into the MSDD. Hence, an iterative A/P detection framework for MSDD-aided DAPSK system was proposed in Section IV-A, which was shown to be capable of achieving a low-complexity near-ML performance. On the other hand, upon the construction of an equivalent multiple-symbol transmission model for the DUSTM-QAM system, we proposed in Section IV-B2 to incorporate the joint detection of the power normalization factor and of the transmitted space-time information symbol into the layered tree search conducted by our newly devised partial SD process, which exploits the properties of the corresponding partial channel matrix, hence resulting in a low-complexity MSDD implementation. In the final part of our treatise, namely in Section V, an in-depth discussion was dedicated to the so-called differential SDMA system, where the multiple access interference was removed by our adaptive differential interference suppression scheme.

B. Design Guideline

- MIMOs circumvent the capacity/power limitation of classic single-antenna-aided systems, since they may be able to increase the achievable throughpot linearly, rather than logarithmically with the transmit power.
- However, the MIMO-capacity degrades in the presence of correlated shadow-fading. Hence the single-antenna-based mobiles, which are sufficiently far apart may form a VAA to circumvent this limitation with the aid of cooperation.
- Another challenge in the design of MIMOs is their channel camplex estimation, since they require the estimation of $(N_{\mathrm{Tx}} \times N_{\mathrm{Rx}})$ links, which is extremely demanding

both in terms of its computational requirements as well as in terms of its potentially excessive pilot overhead. This is particularly so for high Doppler frequencies. These two factors may lead to a performance erosion, which may be mitigated with the aid of low-complexity non-coherent detection aided MIMOs dispensing with channel estimation.

- Indeed, coherent-detection aided VAAs would be even more challanging to design than their classic MIMO counterparts relying on co-located elements, since it is somewhat unrealistic to expect the low-complexity, light-weight MSs to estimate each other's channels, let alone the associated data-security aspects of potential eavesdropping...
- However, the widely recognized impediment of low-complexity non-coherent detection is its typical 3dB performance loss and the potential BER-floor experienced in case of high Doppler frequencies.
- Meanwhile, the need for more flexible compromise between performance and complexity as well as enhanced iteration gain in the context of channel-code-aided iterative receiver has become increasingly urgent for future wireless communications dispensing with channel estimation.
- The joint multiple-symbol based signal processing, such as the MSDD detection technique features prominently on the list of the recent technical advances with a chance of resolving above-mentioned problems at a reasonably low complexity with the aid of sphere decoding mechanism.
- Unfortunately, the direct application of MSDSD for future high-spectrum-efficiency transmissions employing the DAPSK or DUSTM-QAM schemes is prevented by the nonconstant-modulus modulation constellation structure, since it undermines the unitarity of the multiple-symbol transmitted signal matrix.
- Hence, the multiple-symbol based detection may be decoupled for the amplitude and phase of the transmitted DAPSK symbols and an iterative information exchange mechanism may be devised between them for retrieving the performance loss potentially caused by the decoiupling of the A/P detection process.
- As for DUSTM-QAM systems, incorporating a joint detection of the power normalization factor and of the transmitted space-time information symbol into the layered tree search process may be invoked for the sake of a low-complexity implementation, which exploits the properties of the corresponding partial channel matrix.
- On the other hand, the signal separation capability at the receiver of differentially modulated SDMA systems dispensing with channel estimation requires further enhancements in high-Doppler scenarios.
- To this end, inspired by the block-based least-squares algorithm of [95] designed for standard MMSE adaptation, the so-called multiple-symbol DIS scheme based on the MSINR criterion is devised, which is also capable of reducing the filter adaptation overheads and - even more importantly - for facilitating the implementation of the powerful MSDSD.
- In order to further exploit the differential coding gains in the context of our adaptive MS-DIS scheme, a new channel-code-aided three-stage turbo DIS receiver was then proposed, which allowed a beneficial information exchange amongst the concatenated adaptive MS-DIS filter bank, the MSDSD and the channel decoder.
- Finally, a new adaptive-window-duration based MSDSD scheme was conceived, which was further aided by the proposed ALT technique for the sake of achieving significant complexity reductions in the turbo DIS receiver.

C. Future Research

Nonetheless, there are numerous interesting problems associated with the design of differentially modulated wireless communication systems as well as with their multiple-symbol signal processing mechanism, which need further investigation in the future:

1) Achieving further complexity reductions for the MSDSD os conventional differentially detected systems may be a challenging but worthwhile issue to tackle. Amongst a range of interesting ideas proposed recently, the so-called forward/backward-MSDSD (FB-MSDSD) [100] has the potential of reducing the complexity by dividing the original detection interval into forward and backward oriented processes.

2) Recently, the MSDD has been proposed for the double-differential modulation aided system of [101] in order to achieve an enhanced robustness against the frequency variation which distorts the transmitted signal through attenuating its amplitude and introducing a time-varying phase shift to the information symbols. However, a more efficient implementation of the MSDD taking the characteristic of double differential modulation into account may require a further specialized design.

3) The multiuser/multistream interference management is one of the most critical and challenging problems that requires further enhancements in order to design higher-efficiency non-orthogonal differentially modulated cooperative systems, since the channel estimation for all cooperating links beomes significantly more difficult than in their point-to-point direct transmission based counterparts. A possible way forward is to design a joint receiver and cooperative protocol, for example, as proposed in [102].

4) Additionally, scheduling and adaptive rate control is another issue associated with the family of differentially modulated systems based on multiple-symbol signal processing that has to be studied for the sake of achieving a high throughput, while maintaining a reasonably low complexity. To this end, we may seek further solutions dispensing with CSI, while using EXIT-chart-based design techniques [103]. The adaptive window duration based scheme discussed in this treatise may also be taken into account in the design of link adaptation.

5) Finally, The synchronization issues of cooperative systems require substantial further attention.

APPENDIX

Acronyms See Table VI.)

Table VI
ACRONYMS

AF	Amplify-and-Forward
ALT	Apriori-LLR Threshold
AWD	Adaptive Window Duration
BS	Base Station
CDAD	Conventional Differential Amplitude Detection
CDD	Conventional Differential Detection
CDMA	Code-Division Multiple-Access
CDPD	Conventional Differential Phase Detection
CF	Compress-and-Forward
CIR	channel impulse response
CSI	Channel State Information
CTF	Channel Transfer Factor
DAF	Differential Amplify-and-Forward
DAPSK	Differential Amplitude and Phase Shift Keying
DDF	Differential Decode-and-Forward
DF	Decode-and-Forward
DFT	Discrete Fourier Transform
DIS	Differential Interference Suppression
DL	Downlink
DOSTBC	Differential Orthogonal STBC
DPSK	Differential Phase Shift Keying
DUSTM	Differential Unitary Space-Time Modulation
EXIT	EXtrinsic Information Transfer
FD-CTF	Frequency Domain Channel Transfer Factor
FDM	Frequency Divison Multiplexing
IAP-MSDD	Iterative Amplitude/Phase Multiple-Symbol Differential Detector
IAP-MSDSD	Iterative Amplitude/Phase Multiple-Symbol Differential Sphere Detector
ID	Iterative Detection
LMS	Least Mean Square
MAP	Maximum-a-Posteriori
MI	Mutual Information
MIMO	Multiple-Input Multiple-Output
ML	Maximum Likelihood
MMSE	Minimum Mean Square Error
MS	Mobile Station
MSDAD	Multiple-Symbol Differential Amplitude Detector
MSDD	Multiple-Symbol Differential Detection
MSDPD	Multiple-Symbol Differential Phase Detector
MSDSD	Multiple-Symbol Differential Sphere Detection
MS-DSDMA	Multiple-Symbol Differential SDMA
MSINR	Maximum Signal-to-Interference-plus-Noise Ratio
OFDM	Orthogonal Frequency-Division Multiplexing
OFDMA	Orthogonal Frequency-Division Multiple Access
QoE	Quality of End-User Experience
QoS	Quality of Service
RLS	Recursive Least Squares
RS	Relay Station
SC-FDMA	Single-Carrier Frequency-Division Multiple Access
SD	Sphere Detection
SDMA	Spatial-Dvision Multiple Access
SISO	Single-Input Single-Output
SSDD	Soft-Symbol Decision Direct
Star-QAM	Star Quadrature Amplitude Modulation
TD	Time Domain
TDMA	Time-Division Multiple Access
UE	User Equipment
UL	Uplink
VAA	Virtual Antenna Array
WCDMA	Wideband Code-Division Multiple Access

REFERENCES

[1] L. Hanzo, M. Munster, B. J. Choi, and T. Keller, *OFDM and MC-CDMA for Broadband Multi-User Communications, WLANs and Broadcasting*. John Wiley and IEEE Press, 2003.

[2] A. J. Paulraj and T. Kailath, "Increasing capacity in wireless broadcast systems using distributed transmission/directional reception," *US Patent 5 345 599*, 1994.

[3] G. J. Foschini, "Layered space-time architecture for wireless communication in fading environments when using multiple antennas," *Bell Labs Technical Journal*, vol. 2, pp. 41–59, 1996.

[4] G. J. Foschini and M. J. Gans, "On limits of wireless communications in a fading environment when using multiple antennas," *Wireless Personal Communications*, vol. 6, pp. 311–335, Mar. 1998.

[5] N. Chiurtu, B. Rimoldi, and E. Telatar, "On the capacity of multi-antenna Gaussian channels," in *Proc. IEEE International Symposium on Information Theory*, (Washington, DC), p. 53, June 2001.

[6] S. M. Alamouti, "A simple transmit diversity technique for wireless communications," *IEEE J. Sel. Areas Commun.*, vol. 16, pp. 1451–1458, Oct. 1998.

[7] B. Hochwald, T. L. Marzetta, and C. B. Papadias, "A transmitter diversity scheme for wideband CDMA systems based on space-time spreading," *IEEE J. Sel. Areas Commun.*, vol. 19, pp. 48–60, Jan. 2001.

[8] W. F. Su, Z. Safar, and K. J. R. Liu, "Space-time signal design for time-correlated Rayleigh fading channels," *IEEE International Conference on Communications 2003.*, vol. 5, pp. 3175–3179, May 2003.

[9] W. Su and X. G. Xia, "On space-time block codes from complex orthogonal designs," *Wireless Personal Communications*, vol. 25, pp. 1–26, April 2003.

[10] V. Tarokh, H. Jafarkhani, and A. R. Calderbank, "Space-time block codes from orthogonal designs," *IEEE Trans. Inf. Theory*, vol. 45, pp. 1456–1467, July 1999.

[11] G. D. Golden, C. J. Foschini, R. A. Valenzuela, and P. W. Wolniansky, "Detection algorithm and initial laboratory results using V-BLAST space-time communication architecture," *Electronics Letters*, vol. 35, pp. 14–16, Jan. 1999.

[12] H. Lee, B. Lee, and I. Lee, "Iterative detection and decoding with an improved v-BLAST for MIMO-OFDM systems," *IEEE J. Sel. Areas Commun.*, vol. 24, pp. 504–513, Mar. 2006.

[13] D. Gesbert, M. Shafi, D. shan Shiu, P. J. Smith, and A. Naguib, "From theory to practice: an overview of MIMO space-time coded wireless systems," *IEEE J. Sel. Areas Commun.*, vol. 21, pp. 281–302, Apr. 2003.

[14] J. Mietzner, R. Schober, L. Lampe, W. H. Gerstacker, and P. A. Hoeher, "Multiple-antenna techniques for wireless communications - a comprehensive literature survey," *IEEE Commun. Surveys & Tutorials*, vol. 11, pp. 87–105, second quater 2009.

[15] T. S. Rappaport, *Wireless Communications Principles and Practise*. Pearson Education Asia Limited and Publishing House of Electronics Industry, second ed., 2002.

[16] T. Cover and A. E. Gamal, "Capacity theorems for the relay channel," *IEEE Trans. Inf. Theory*, vol. 25, pp. 572–584, Sept. 1979.

[17] R. Pabst, "Relay-based deployment concepts for wireless and mobile broadband radio," *IEEE Commun. Mag.*, vol. 42, pp. 80–89, Sept. 2004.

[18] D. Soldani and S. Dixit, "Wireless relays for broadband access," *IEEE Commun. Mag.*, vol. 46, pp. 58–66, Mar. 2008.

[19] A. Sendonaris, E. Erkip, and B. Aazhang, "User cooperation diversity. part I: System description," *IEEE Trans. Commun.*, vol. 51, pp. 1927–1938, Nov. 2003.

[20] A. Sendonaris, E. Erkip, and B. Aazhang, "User cooperation diversity. part II: Implementation aspects and performance analysis," *IEEE Trans. Commun.*, vol. 51, pp. 1939–1948, Nov. 2003.

[21] J. N. Laneman, D. N. C. Tse, and G. W. Wornell, "Cooperative diversity in wireless networks: Efficient protocols and outage behavior," *IEEE Trans. Inf. Theory*, vol. 50, pp. 3062–3080, Dec. 2004.

[22] K. G. Seddik, A. K. Sadek, W. Su, and K. J. R. Liu, "Outage analysis and optimal power allocation for multinode relay networks," *IEEE Signal Process. Lett.*, vol. 14, pp. 377–380, June 2007.

[23] G. Kramer, M. Gastpar, and P. Gupta, "Cooperative strategies and capacity theorems for relay networks," *IEEE Trans. Wireless Commun.*, vol. 51, pp. 3037–3063, Sept. 2005.

[24] S. Simoens, O. Muoz-Medina, J. Vidal, and A. D. Coso, "Compress-and-forward cooperative mimo relaying with full channel state information," *IEEE Trans. Wireless Commun.*, vol. 58, pp. 781–791, Feb. 2010.

[25] K. Etemad, "Overview of mobile WiMAX technology and evolution," *IEEE Commun. Mag.*, vol. 46, pp. 31–40, Oct. 2008.

[26] K. Etemad, "Multisite filed trial for LTE and advanced concepts," *IEEE Commun. Mag.*, vol. 47, no. 2, pp. 92–98, 2009.

[27] P. Hoher, "TCM on frequency-selective land-mobile fading channels," *5th International Workshop Digital Communications, B. V. M. Luise and E. Biglieri, Eds. Pisa, Italy: Elsevier*, pp. 8–12, 1991.

[28] Y. Wu and M. Patzold, "Performance analysis of cooperative communication systems with imperfect channel estimation," *IEEE International Conference on Communications (ICC'09)*, June 2009.

[29] S. Han, S. Ahn, E. Oh, and D. Hong, "Effect of channel-estimation

error on ber performance in cooperative transmission," *IEEE Trans. Veh. Technol.*, vol. 58, pp. 2083–2088, May 2009.

[30] J. G. Proakis, *Digital Communications*. 4th edition, New York, NY: Mc-Graw-Hill, 2000.

[31] T. Himsoon, W. P. Siriwongpairat, W. Su, and K. J. R. Liu, "Differential modulations for multinode cooperative communications," *IEEE Trans. Signal Process.*, vol. 56, pp. 2941–2956, July 2008.

[32] T. Himsoon, W. P. Siriwongpairat, W. Su, and K. J. R. Liu, "Differential modulation with threshold-based decision combining for cooperative communications," *IEEE Trans. Signal Process.*, vol. 55, pp. 3905–3923, July 2007.

[33] W. Su, F. Chen, D. A. Pados, and J. D. Matyjas, "The outage probability and optimum power assignment for differential amplify-and-forward relaying," *IEEE International Conference on Communications*, pp. 1–5, May 2010.

[34] Q. Zhao and H. Li, "Performance of differential modulation with wireless relays in Rayleigh fading channels," *IEEE Commun. Lett.*, vol. 9, pp. 343–345, Apr. 2005.

[35] Q. Zhao and H. Li, "Differential modulation for cooperative wireless systems," *IEEE Trans. Signal Process.*, vol. 55, pp. 2273–2283, May 2007.

[36] T. Cui, F. Gao, and C. Tellambura, "Differential modulation for two-way wireless communications: a perspective of differential network coding at the physical layer," *IEEE Trans. Commun.*, vol. 57, pp. 2977–2987, Oct. 2009.

[37] L. Hanzo, Y. Akhtman, L. Wang, and M. Jiang, *MIMO-OFDM for LTE, WIFI and WIMAX: Coherent versus Non-Coherent and Cooperative Turbo-Transceivers*. John Wiley and IEEE Press, 2010.

[38] L. Wang and L. Hanzo, "Dispensing with channel estimation: Differentially modulated cooperative wireless communications," in *IEEE Commun. Surveys & Tutorials*, vol. 14, pp. 836 – 857, 2012.

[39] L. Wang, L. Kong, S. X. Ng, and L. Hanzo, "Code-rate-optimized differentially modulated near-capacity cooperation," in *IEEE Trans. Commun.*, vol. 59, pp. 2185 – 2195, Aug. 2011.

[40] W. T. Webb, L. Hanzo, and R. Steele, "Bandwidth efficient QAM schemes for Rayleigh fading channels," *IEE Proceedings I, Communications, Speech and Vision*, vol. 138, pp. 169–175, June 1991.

[41] H. Rohling and V. Engels, "Differential amplitude phase shift keying (DAPSK) - a new modulation method for DTVB," *Proc. International Broadcasting Convention*, pp. 102–108, 1995.

[42] F. Adachi and M. Sawahashi, "Decision feedback differential detection of differentially encoded 16APSK signals," *IEEE Trans. Commun.*, vol. 44, pp. 416–418, Apr. 1996.

[43] B. M. Hochwald and W. Sweldens, "Differential unitary space-time modulation," *IEEE Trans. Commun.*, vol. 48, no. 12, pp. 2041–2052, 2000.

[44] B. L. Hughes, "Differential space-time modulation," *IEEE Trans. Inf. Theory*, vol. 46, pp. 2567–2578.

[45] G. Wang, Y. Zhang, and M. Amin, "Differential distributed space-time modulation for cooperative networks," *IEEE Trans. Wireless Commun.*, vol. 5, pp. 3097–3108, Nov. 2006.

[46] Y. Jing and H. Jafarkhani, "Distributed differential space-time coding for wireless relay networks," *IEEE Trans. Commun.*, vol. 56, pp. 1092–1100, July 2008.

[47] F. Oggier and E. Lequeu, "Differential distributed cayley space-time codes," *IEEE Trans. Wireless Commun.*, vol. 8, pp. 3808–3814, July 2009.

[48] S. Yiu, R. Schober, and L. Lampe, "Differential distributed space-time block coding," *IEEE Pacific Rim Conference on Communications, Computers and Signal Processing*, pp. 53–56, 2005.

[49] V. Tarokh and H. Jafarkhani, "A differential detection scheme for transmit diversity," *IEEE J. Sel. Areas Commun.*, vol. 18, no. 7, pp. 1169–1174, 2000.

[50] A. Shokrollahi, B. Hassibi, B. M. Hochwald, and W. Sweldens, "Representation theory for high-rate multiple-antenna code design," *IEEE Trans. Inf. Theory*, vol. 47, no. 6, pp. 2335–2367, 2001.

[51] B. Hassibi and B. M. Hochwald, "Cayley differential unitary space-time codes," *IEEE Trans. Inf. Theory*, vol. 48, no. 6, pp. 1485–1503, 2002.

[52] L. Z. Zheng and D. N. C. Tse, "Communication on the grassmann manifold: a geometric approach to the noncoherent multiple-antenna channel," *IEEE Trans. Inf. Theory*, vol. 48, pp. 359–383, Feb. 2002.

[53] S. H. Nam, C. S. Hwang, J. Chung, and V. Tarokh, "Differential space time block codes using QAM for four transmit antennas," in *IEEE International Conference on Communications*, vol. 2, pp. 952–956, June 2004.

[54] Y. Zhu and H. Jafarkhani, "Differential modulation based on quasi-orthogonal codes," *IEEE Trans. Wireless Commun.*, vol. 4, no. 6, pp. 3005–3017, 2005.

[55] F. Oggier, "Cyclic algebras for noncoherent differential space-time coding," *IEEE Trans. Inf. Theory*, vol. 53, pp. 3053–3065, September 2007.

[56] I. Stewart, *Galois Theory*. London, UK: Chapman and Hall, 1989.

[57] G. Wang, , Y. Zhang, and M. Amin, "Differential distributed space-time modulation for cooperative networks," *IEEE Trans. Wireless Commun.*, vol. 5, pp. 3097 – 3108, Nov. 2006.

[58] S. Yiu, R. Schober, and L. Lampe, "Distributed space-time block coding," *IEEE Trans. Commun.*, vol. 54, pp. 1195 – 1206, 2006.

[59] Y. Jing and H. Jafarkhani, "Distributed differential space-time coding for wireless relay networks," *IEEE Trans. Commun.*, vol. 56, pp. 1092 – 1100, 2008.

[60] G. S. Rajan and B. S. Rajan, "Algebraic distributed differential space-time codes with low decoding complexity," *IEEE Trans. Wireless Commun.*, vol. 7, pp. 3962 – 3971, Oct. 2008.

[61] F. Oggier and E. Lequeu, "Differential distributed cayley space-time codes," *IEEE Trans. Wireless Commun.*, vol. 8, pp. 3808 – 3814, 2009.

[62] Z. Gao and H. Q. L. K. J. R. Liu, "Differential space-time network coding for multi-source cooperative communications," *IEEE Trans. Commun.*, vol. 59, pp. 3146 – 3157, Nov. 2011.

[63] Q. Huo, L. Song, Y. Li, and B. Jiao, "A distributed differential space-time coding scheme with analog network coding in two-way relay networks," *IEEE Trans. Signal Process.*, vol. 60, pp. 4998 – 5004, Sept. 2012.

[64] P. Dayal, M. Brehler, and M. K. Varanasi, "Leveraging coherent space-time codes for noncoherent communication via training," *IEEE Trans. Inf. Theory*, vol. 50, pp. 2058–2080, Sept. 2004.

[65] G. Farhadi and N. Beaulieu, "Fixed relaying versus selective relaying in multi-hop diversity transmission systems," *IEEE Trans. Commun.*, vol. 58, pp. 956–965, Mar. 2010.

[66] W. W. Peterson and D. T. Brown, "Cyclic codes for error detection," *Proc. Institute of Radio Engineers*, vol. 49, pp. 228–235, Jan. 1961.

[67] T. Himsoon, W. Su, and K. J. R. Liu, "Differential transmission for amplify-and-forward cooperative communications," *IEEE Signal Process. Lett.*, vol. 12, pp. 597–600, Sept. 2005.

[68] L. Wang and L. Hanzo, "The amplify-and-forward cooperative uplink using multiple-symbol differential sphere-detection," *IEEE Signal Proc. Lett.*, vol. 16, pp. 913–916, Oct. 2009.

[69] V. Pauli and L. Lampe, "Multiple-symbol differential sphere decoding for unitary space-time modulation," *IEEE Global Telecommunications Conference*, vol. 3, p. 6, Nov. 2005.

[70] Y. Liang and V. V. Veeravalli, "Capacity of noncoherent time-selective rayleigh-fading channels," *IEEE Trans. Inf. Theory*, vol. 50, pp. 3095–3110, Dec. 2004.

[71] U. Fincke and M. Pohst, "Improved methods for calculating vectors of short length in a lattice, including a complexity analysis," *Mathematics of Computation*, vol. 44, pp. 463–471, April 1985.

[72] E. Viterbo and J. Boutros, "A universal lattice code decoder for fading channels," *IEEE Trans. Inf. Theory*, vol. 45, pp. 1639–1642, July 1999.

[73] L. Lampe, R. Schober, V. Pauli, and C. Windpassinger, "Multiple-symbol differential sphere decoding," *IEEE Trans. Commun.*, vol. 12, pp. 1981–1985, Dec. 2005.

[74] D. Divsalar and M. K. Simon, "Multiple-symbol differential detection of MPSK," *IEEE Trans. Commun.*, vol. 38, pp. 300–308, Mar. 1990.

[75] D. Divsalar and M. K. Simon, "Maximum-likelihood differential detection of uncoded and trellis-coded amplitude phase modulation over awgn and fading channels–metrics and performance," *IEEE Trans. Commun.*, vol. 42, pp. 76–89, Jan. 1994.

[76] R. A. Horn and C. R. Johnson, *Matrix Analysis*. Cambridge University Press, 1985.

[77] M. O. Damen, K. Abed-Meraim, and J. C. Belfiore, "Generalised sphere decoder for asymmetrical space-time communication architecture," *Electronics Letters*, vol. 36, pp. 166–167, Jan. 2000.

[78] T. Cui and C. Tellambura, "An efficient generalized sphere decoder for rank-deficient MIMO systems," *IEEE Commun. Lett.*, vol. 9, pp. 423–425, May 2005.

[79] J. Jalden and B. Ottersten, "On the complexity of sphere decoding in digital communications," *IEEE Trans. Signal Process.*, vol. 53, pp. 1474–1484, 2005.

[80] J. Akhtman and L. Hanzo, "An optimized-hierarchy-aided maximum likelihood detector for MIMO-OFDM," *IEEE 63rd Vehicular Technology Conference, VTC 2006-Spring*, vol. 3, pp. 1526–1530, 2006.

[81] I. Motedayen-Aval, A. Krishnamoorthy, and A. Anastasopoulos, "Optimal joint detection/estimation in fading channels with polynomial complexity," *IEEE Trans. Inf. Theory*, vol. 53, pp. 209–223, 2007.

[82] V. Pauli, L. Lampe, R. Schober, and K. Fukuda, "Multiple-symbol differential detection based on combinatorial geometry," *IEEE Trans. Commun.*, vol. 56, pp. 1596–1600, 2008.
[83] L. Hanzo, S. X. Ng, W. Webb, and T. Keller, *Quadrature Amplitude Modulation: From Basics to Adaptive Trellis-Coded, Turbo-Equalised and Space-Time Coded OFDM, CDMA and MC-CDMA Systems*. Wiley-Blackwell, 2004.
[84] V. Engels and H. Rohling, "Multilevel differential modulation techniques (64-dapsk) for multicarrier transmission systems," *European Trans. Telecommunications*, vol. 6, pp. 633–640, Nov. 1995.
[85] H. Rohling and V. Engels, "Differential amplitude phase shift keying (DAPSK) a new modulation method for DVBT," *International Broadcasting Convention*, pp. 102–108, Sept. 1995.
[86] A. Song, G. Wang, W. Su, and X. G. Xia, "Unitary space-time codes from Alamouti's scheme with APSK signals," *IEEE Trans. Wireless Commun.*, vol. 3, pp. 2374–2384, Nov. 2004.
[87] C. S. Hwang, S. H. Nam, J. Chung, and V. Tarokh, "Differential space time block codes using nonconstant modulus constellations," *IEEE Trans. Signal Process.*, vol. 51, no. 11, pp. 2955–2964, 2003.
[88] F. Adachi and M. Sawahashi, "Performance analysis of various 16 level modulation schemes under Rayleigh fading," *Electronics Letters*, vol. 28, pp. 1579–1581, Aug. 1992.
[89] M. Machida, S. Handa, and S. Oshita, "Multiple-symbol differential detection of APSK based on MAP criterion," *IEEE Global Telecommunications Conference*, vol. 5, pp. 2740–2744, Nov. 1998.
[90] V. Pauli, L. Lampe, and R. Schober, ""Turbo DPSK" using soft multiple-symbol differential sphere decoding," *IEEE Trans. Inf. Theory*, vol. 52, no. 4, pp. 1385–1398, 2006.
[91] K. Ishibashi, H. Ochiai, and R. Kohno, "Low-complexity bit-interleaved coded DAPSK for Rayleigh-fading channels," *IEEE J. Sel. Areas Commun.*, vol. 23, pp. 1728–1738, Sept. 2005.
[92] A. Ashikhmin, G. Kramer, and S. ten Brink, "Extrinsic information transfer functions: model and erasure channel properties," *IEEE Trans. Inf. Theory*, vol. 50, pp. 2657–2673, Nov. 2004.
[93] L. Lampe and R. Fischer, "Comparison and optimization of differentially encoded transmission on fading channels," *in Proc. 3rd Int. Symp. Power-Line Communications (ISPLC)*, 1999.
[94] T. Weber, A. Sklavos, and M. Meurer, "Imperfect channel-state information in MIMO transmission," *IEEE Trans. Commun.*, vol. 54, pp. 543–552, Mar. 2006.
[95] H. V. Poor and G. W. Wornell, *Wireless Communications: Signal Processing Perspectives*. Prentice Hall PTR, 1998.
[96] S. K. Cheung and R. Schober, "Differential spatial multiplexing," *IEEE Trans. Wireless Commun.*, vol. 5, pp. 2127–2135, Aug. 2006.
[97] H.-J. Su and E. Geraniotis, "Maximum signal-to-noise ratio array processing for space-time coded systems," *IEEE Trans. Commun.*, vol. 50, pp. 1419–1422, Sept. 2002.
[98] L. Wang and L. Hanzo, "Differential interference suppression for SDMA-OFDM based on joint multiple-symbol filtering and detection," *IEEE Trans. Veh. Technol.*, vol. 60, pp. 4656–4662, Nov. 2011.
[99] J. Yang, F. Yang, H.-S. Xi, W. Guo, and Y. Sheng, "Robust adaptive modified newton algorithm for generalized eigendecomposition and its application," *EURASIP J. Advances in Signal Processing*, vol. 2007, pp. 1–10, June 2007.
[100] C.-C. Lo and S.-L. Su, "Combining of forward and backward multiple-symbol differential sphere decoding for turbo coded system," *IEEE Vehicular Technology Conference (VTC'10-Spring)*, May 2010.
[101] A. M. Rabiei and N. C. Beaulieu, "Frequency offset invariant multiple symbol differential detection of mpsk," *IEEE Trans. Commun.*, vol. 59, pp. 652 – 657, Mar. 2011.
[102] L. Li, L. Wang, and L. Hanzo, "Differential interference suppression aided three-stage concatenated successive relaying," *IEEE Trans. Commun.*, vol. 60, pp. 2146 – 2155, Aug. 2012.
[103] S. Ibi, T. Matsumoto, R. Thoma, S. Sampei, and N. Morinaga, "Exit chart-aided adaptive coding for multilevel bicm with turbo equalization in frequency-selective mimo channels," *IEEE Trans. Veh. Technol.*, vol. 56, pp. 3757–3769, Nov. 2007.

Li Wang (S'09-M'10) was born in Chengdu, China, in 1982. He received his BEng degree in Information Engineering from Chengdu University of Technology (CDUT), Chengdu, China, in 2005 and his MSc degree with distinction in Radio Frequency Communication Systems from the University of Southampton, UK, in 2006. Between October 2006 and January 2010 he was pursuing his PhD degree in the Communications Group, School of Electronics and Computer Science, University of Southampton, and meanwhile he participated in the Delivery Efficiency Core Research Programme of the Virtual Centre of Excellence in Mobile and Personal Communications (Mobile VCE). Upon completion of his PhD in January 2010 he conducted research as a Senior Research Fellow in the School of Electronics and Computer Science at the University of Southampton. During this period he was involved in Project #7 of the Indian-UK Advanced Technology Centre (IU-ATC): advanced air interface technique for MIMO-OFDM and cooperative communications. In March 2012 he joined the R&D center of Huawei Technologies in Stockholm, Sweden, working as Senior Engineer of Baseband Algorithm Architecture. He has published over 30 research papers in IEEE/IET journals and conferences, and he also co-authored one John Wiley/IEEE Press book. He has broad research interests in the field of wireless communications, including PHY layer modeling, link adaptation, cross-layer system design, multi-carrier transmission, MIMO techniques, CoMP, channel coding, multi-user detection, non-coherent transmission techniques, advanced iterative receiver design and adaptive filter.

Li Li received the B.Eng. degree in information engineering from the University of Electronic Science and Technology of China (UESTC), Chengdu, China, in 2006 and the M.Sc. degree with distinction in wireless communications from the University of Southampton, Southampton, U.K., in 2009. He is currently working towards the Ph.D. degree with the Research Group of Communications, Signal Processing and Control, School of Electronics and Computer Science, University of Southampton, Southampton, U.K., and participating in the European Union Concerto project. His research interests include channel coding, iterative detection, non-coherent transmission technologies, cooperative communications, interference suppression techniques and network coding.

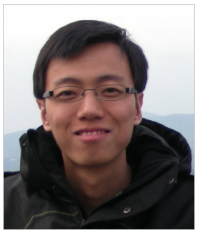

Chao Xu (S'09) received the B.Eng. degree from Beijing University of Posts and Telecommunications, Beijing, China, and the B.Sc.(Eng) (first-class honors) from Queen Mary, University of London, London, UK, in 2008, both in Telecommunications Enginneering with Management and both through a Sino-UK joint degree program. He received the M.Sc. degree (with distinction) in radio frequency communication systems from the University of Southampton, Southampton, UK, in 2009. He is currently working towards the PhD degree with the Research Group of Commmunications, Signal Processing and Control, School of Electronics and Computer Science, University of Southampton. His research interests include reduced-complexity multiple-input-multiple-output design, noncoherent spacetime modulation detection, extrinsic-information-transfer-chart-aided turbo detection, and cooperative communications.

Mr. Xu was awarded the 2009 Best M.Sc. Student in Broadband and Mobile Communication Networks by the IEEE Communications Society (United Kingdom and Republic of Ireland Chapter), and the 2013 Chinese Government Award for Outstanding Self-Financed Students Abroad.

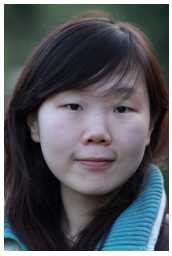

Dandan Liang (S'09) received her B.Eng. degree (First class) in electronic science and technology from the PLA Information Engineering University, Zhengzhou, China, in 2008. She received her M.Sc. degree (First class) in radio frequency communication systems and Ph.D. degree in wireless communications from the University of Southampton, UK, in 2009 and 2013, respectively. Her research interests include adaptive coded modulation, coded modulation, non/coherent modulation detection, iterative detection, networking coding, cooperative communications as well as wireless-optical fiber communications.

Soon Xin Ng (S'99-M'03-SM'08) received the B.Eng. degree (First class) in electronics engineering and the Ph.D. degree in wireless communications from the University of Southampton, Southampton, U.K., in 1999 and 2002, respectively. From 2003 to 2006, he was a postdoctoral research fellow working on collaborative European research projects known as SCOUT, NEWCOM and PHOENIX. Since August 2006, he has been a member of academic staff in the School of Electronics and Computer Science, University of Southampton. He is involved in the OPTIMIX and CONCERTO European projects as well as the IU-ATC and UC4G projects. He is currently a senior lecturer at the University of Southampton.

His research interests include adaptive coded modulation, coded modulation, channel coding, space-time coding, joint source and channel coding, iterative detection, OFDM, MIMO, cooperative communications, distributed coding, quantum error correction codes and joint wireless-and-optical-fiber communications. He has published over 160 papers and co-authored two John Wiley/IEEE Press books in this field. He is a Senior Member of the IEEE, a Chartered Engineer and a Fellow of the Higher Education Academy in the UK.

Lajos Hanzo FREng, FIEEE, FIET, Fellow of EURASIP, DSc received his degree in electronics in 1976 and his doctorate in 1983. In 2009 he was awarded the honorary doctorate "Doctor Honoris Causa" by the Technical University of Budapest. During his 35-year career in telecommunications he has held various research and academic posts in Hungary, Germany and the UK. Since 1986 he has been with the School of Electronics and Computer Science, University of Southampton, UK, where he holds the chair in telecommunications. He has successfully supervised 80 PhD students, co-authored 20 John Wiley/IEEE Press books on mobile radio communications totalling in excess of 10 000 pages, published 1300 research entries at IEEE Xplore, acted both as TPC and General Chair of IEEE conferences, presented keynote lectures and has been awarded a number of distinctions. Currently he is directing a 100-strong academic research team, working on a range of research projects in the field of wireless multimedia communications sponsored by industry, the Engineering and Physical Sciences Research Council (EPSRC) UK, the European IST Programme and the Mobile Virtual Centre of Excellence (VCE), UK. He is an enthusiastic supporter of industrial and academic liaison and he offers a range of industrial courses. He is also a Governor of the IEEE VTS. During 2008 - 2012 he was the Editor-in-Chief of the IEEE Press and a Chaired Professor also at Tsinghua University, Beijing. His research is funded by the European Research Council's Senior Research Fellow Grant. For further information on research in progress and associated publications please refer to http://www-mobile.ecs.soton.ac.uk.